Review

Heterostructures construction on TiO$_2$ nanobelts: A powerful tool for building high-performance photocatalysts

Xiaofei Zhang [a,1], Yana Wang [a,1], Baishan Liu [b], Yuanhua Sang [a,*], Hong Liu [a,b,*]

[a] State Key Laboratory of Crystal Materials, Shandong University, Jinan 250100, PR China
[b] Jiaxing Rejdue Environmental Technology Co., Ltd., Jiaxing 314006, PR China

ARTICLE INFO

ABSTRACT

Semiconductor photocatalysis is a promising approach to combat both environmental pollution and the global energy shortage. Advanced TiO$_2$-based photocatalysts with novel photoelectronic properties are benchmark materials that have been pursued for their high solar energy conversion efficiency. Among the different morphological TiO$_2$ nanostructures, TiO$_2$ nanobelts (NBs) attract more attention due to their unique physical properties and ideal 1D ribbon-like morphology that is favorable for constructing heterostructures by assembling second-phase nanoparticles on the surface of the NBs. A large number of studies have proven that well-designed TiO$_2$ NB heterostructures can not only broaden the photocatalytically active light band of TiO$_2$ but also enhance the light absorption performance and the photo-induced carrier separation ability. The TiO$_2$ NB heterostructure has become a versatile and powerful tool for building high-performance TiO$_2$-based photocatalysts, which has stimulated intense research activities focused on the growth, properties, and applications of the 1D TiO$_2$ NB and its heterostructures. This review attempts to cover all these aspects, including the underlying principles and key functional features of TiO$_2$ NBs and TiO$_2$ NB heterostructures in a comprehensive way and also discuss the prospects of this type of novel hybrid photocatalyst.

© 2016 Elsevier B.V. All rights reserved.

Contents

* Corresponding authors at: State Key Laboratory of Crystal Materials, Shandong University, Jinan, 250100, PR China
  E-mail addresses: sangyh@sdu.edu.cn (Y. Sang), hongliu@sdu.edu.cn (H. Liu).
[1] These authors contributed equally to this work. The author order was determined by coin toss.

1. Introduction

The world is facing two major challenges at the moment: environmental pollution and energy shortage. Semiconductor photocatalysis is a promising approach to combat both of these challenges. Potential applications of photocatalysis include photodegradation of hazardous substances [1,2], photocatalytic water splitting [3,4], artificial photosynthesis for fuel production [5–7], photo-induced super-hydrophilicity [8], and photoelectrochemical conversion [9,10]. Semiconductor materials are the key factors in photocatalysis reactions. Among these semiconductors, TiO$_2$ is the earliest and best-studied photocatalyst with a very high ultraviolet (UV) light activity, and P25 (a TiO$_2$ nanoparticle with approximately 80 wt% anatase and 20 wt% rutile) [11,12] is the most popular commercial photocatalyst product. Unfortunately, TiO$_2$ does not possess photocatalytic properties under visible light, which limits its application when using solar light, which has an energy distribution of less than 5% for UV light, approximately 40% for visible light, and more than 50% for infrared (IR) light [11]. Because the ultimate objective of photocatalysis is the efficient utilization and conversion of solar light, many visible-light photocatalysts, such as CdS [13,14], CdSe [15], InP [16], GaZnON [17], WO$_3$ [18], Ag$_2$O [19], Ag$_2$S [20], Cu$_2$O [21], Bi$_2$MoO$_6$ [22] and Bi$_2$WO$_6$ [23], have been developed. However, all of the existing photocatalysts have some common shortcomings: 1) a narrow light spectrum for photocatalytic activity limited to a typical light spectrum range, causing low efficiency in the utilization of sunlight; and 2) the photo-induced charge carriers in single-crystalline nanostructured materials recombine easily, causing a low production of effective charge carriers and then a decrease in the photocatalytic efficiency. Overcoming these disadvantages is a huge challenge that researchers must face.

It is well accepted that an excellent photocatalyst should have the following characteristics: 1) more active photocatalytic facets; 2) a broad absorption spectrum; and 3) a means of facilitating the separation of photo-induced charge carriers [11]. As mentioned above, TiO$_2$ is the first photocatalyst with an excellent UV-light photocatalytic property [24]. So far, many researchers have made significant progress by using TiO$_2$-based photocatalysts to achieve a high photocatalytic property [25–28]. In terms of increasing the active facets, by controlling the growth process of TiO$_2$ nanocrystals to enable the exposure of more highly active facets, researchers can increase the proportion of the active surface and improve the photocatalytic efficiency [29–31]. To broaden the optical absorption spectrum, cationic or anionic dopants [32], and metal nanoparticles created by a primitive plasma resonance absorption process [33,34] are used to extend the absorption spectra of TiO$_2$ to the visible and even the infrared region. To improve the separation of the photo-induced carriers, energy band matching of the two crystalline TiO$_2$ phases (anatase and rutile) can be used to realize a directional movement of photo-generated carriers and enable their separation, which can enhance the photocatalytic efficiency [35].

However, the above approaches are associated with certain difficulties or limitations in obtaining TiO$_2$ nanoparticles with high photocatalytic performance. For example, although the exposed facets of the semiconductor nano/microcrystals can be controlled to achieve a high proportion of the active surface area, the well-crystallized nano/microcrystals are generally larger in size than granular nanoparticles, and the amount of the active surface per unit mass is not impressive. In addition, the complexity and high cost of controlling the growth of the crystal faces restricts these methods to the theoretical side of research. Anion- and cation-doped TiO$_2$ nanoparticles can obtain visible light catalytic properties through the defects in their energy levels [36], but two shortcomings exist. One is that the defects reduce the intrinsic excellent UV catalytic activity of the TiO$_2$ nanoparticles themselves [37]; the other is that the visible light photocatalytic properties of the TiO$_2$ nanoparticles will decrease during the photocatalysis process due to the recovering of the defects, which limits both their performance and practical application. Band structure matching of the two TiO$_2$ phases to achieve the efficient separation of photo-induced carriers is a very valuable means of improving the performance of TiO$_2$ nanoparticles, and it has been successfully applied in the famous commercial photocatalyst P25. It is consistently found that the valence band maximum of rutile is 0.7 ± 0.1 eV above that of anatase [38]. Therefore, electrons (e$^-$) easily transfer from rutile to anatase, and holes (h$^+$) move to the rutile phase in the process of photocatalysis, thus resulting in highly efficient photocatalysis. Unfortunately, P25 nanoparticles are too small to be removed/collected from the reaction system after degradation of the organic pollutant. The cost of operation of a high-speed centrifuge to recycle P25 after the photocatalytic process is even higher than the cost of purchasing the P25 [11]. In addition, TiO$_2$ nanoparticles can be integrated with other semiconductor nanoparticles to form heterostructures; this can improve the photo-induced carrier based on the band-matching principles. In a similar manner, TiO$_2$ nanoparticles can be combined with visible light photocatalytic nanoparticles to broaden the spectrum for photocatalysis. However, the heterostructures based on TiO$_2$ nanoparticles tend to form core-shell structures or random aggregates of mixed particles

during the preparation process of heterogeneous structures due to the small size of the TiO_2 nanoparticles. As a result, for a TiO_2-based visible light photocatalytic semiconductor heterostructure, not only do the separated charges easily accumulate in the core during the photocatalysis process but the visible light photocatalysts on the shell may block the UV light from entering into the TiO_2 core, causing a reduction in the photocatalytic performance. Therefore, the design and preparation of TiO_2-based heterogeneous photocatalysts with a wide absorption spectrum and high efficiency are still popular areas in the investigation of photocatalysis.

In recent years, TiO_2 NBs have received widespread attention as potentially recyclable photocatalysts due to their high degree of crystallization, unique morphology, carrier localization, high migration in the axial direction, and other characteristics [39]. TiO_2 NBs have immeasurable application prospects in photocatalysis [11]. However, their disadvantages are also obvious: smaller active surfaces, a narrow photocatalytically active spectrum limited to the UV-light region, and a high recombination ratio of photo-induced carriers, which inhibits their practical photocatalysis application [40].

Fortunately, TiO_2 NBs have a special ribbon-like morphology, which endows them with a very large surface area for operation. The plain surface of TiO_2 NBs can be used as a platform to assemble a variety of different nanoparticles to form nanoheterostructures. Through rational design and controllable synthesis, TiO_2 NBs surface heterostructures (abbreviated as TiO_2 NSHs) not only express the intrinsic properties of the second phase but also retain the photocatalytic properties of TiO_2. The application of the principles of bandgap design and other semiconductor surface heterostructure design principles in TiO_2 NSHs can achieve photocatalysts with high efficiencies and broad absorption spectra. The photocatalytic performance of heterostructures in a broad absorption spectrum can be significantly superior to that of single-phase photocatalysts. Therefore, in recent years, photocatalysts based on TiO_2 NB heterostructures have received much attention all over the world, and a variety of TiO_2 NSHs with high photocatalytic performance have shown great application prospects in pollutant degradation and water splitting for hydrogen generation [40]. TiO_2 NSHs have become a powerful tool for the design and preparation of high-performance photocatalysts, which provides a new strategy for building photocatalysts needed in solar energy driven photodegradation of pollutants for environmental engineering, water-splitting for hydrogen generation, and other chemical reaction based on photocatalysis.

In this paper, the recent progress in the research on photocatalysts based on TiO_2 NSHs is comprehensively reviewed. The focus here is on the design principles, synthesis methods, structure characteristics and photocatalytic properties of the TiO_2 NSHs. To improve the readers' understanding of TiO_2 NSHs, the structure, synthesis methods and basic properties of TiO_2 NBs are briefly introduced at the beginning of the article.

2. Preparation and basic properties of TiO_2 NBs

TiO_2 has four main crystalline polymorphs, namely, anatase, rutile, brookite and TiO_2(B). Anatase phase [41] and anatase-based biphasic TiO_2 NBs have been widely investigated in photocatalysis because of their more favorable catalytic properties caused by a synergistic effect between the different polymorphs [42,43]. Herein, we will mainly focus on the synthesis methods, structural characteristics, and the properties of the anatase TiO_2 NBs synthesized via the alkali-hydrothermal process, which we have extensively investigated for the past 8 years.
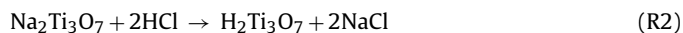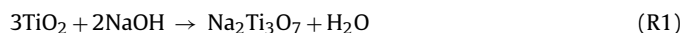
2.1. Synthesis methods for the preparation of TiO_2 NBs

There are several methods to synthesize TiO_2 NBs. The size, degree of crystallization, phase composition, and primary exposed facets of the NBs depend strongly on the synthesis methods. Herein, we mainly discuss hydrothermal and solvothermal methods and the TiO_2 NBs they produce.

2.1.1. Hydrothermal methods

As the most popular method for the synthesis of TiO_2 nanostructures, the hydrothermal process effectively contributes to the formation of well-crystallized TiO_2 NBs. Several chemicals can be used as Ti resources in this process, such as titanium dioxide nanoparticles [44], titanium chloride ($TiCl_4$) [45], Ti foils [46] and titanium butoxide ($Ti(OBu)_4$) [47]. In fact, the hydrothermal method is normally related to hydroxide assistance and follows other treatments to obtain TiO_2 NBs, so it is referred to as the alkali-hydrothermal based method and abbreviated as the hydrothermal method. To obtain single-phase TiO_2 NBs via the alkali-hydrothermal process, some researchers choose P25 as the Ti precursor in the synthesis process because the very small size of the TiO_2 nanoparticles can ensure a uniform morphology of the TiO_2 NBs. Normally, for the hydrothermal method, the three essential steps are the alkali-hydrothermal process, ion exchange and annealing. Typically, 0.1 g of P25 powder is dispersed uniformly in 20 mL of 10 M NaOH aqueous solution, followed by an alkali-hydrothermal treatment at 180–200 °C in a 25 mL Teflon-lined autoclave for 24–72 h and subsequent air-cooling to room temperature [11]. The obtained powders are then washed thoroughly with distilled water and collected by a filtration process to obtain $Na_2Ti_3O_7$ NBs. The ion-exchange process is then performed by immersing $Na_2Ti_3O_7$ NBs in 0.1 M HCl for 24 h with continuous magnetic stirring under ambient conditions to obtain $H_2Ti_3O_7$ NBs. After being annealed at 500–600 °C, the $H_2Ti_3O_7$ NBs can transform to anatase TiO_2 NBs and still retain their belt-like morphology. The proposed underlying mechanism is that the TiO_2 nanoparticles first dissolve in the concentrated alkali solution and then recrystallize during the hydrothermal process, through which $Na_2Ti_3O_7$ NBs tend to form with a layered nanostructure, as illustrated in Fig. 1a. Generally, the thickness of the NBs is about 20–40 nm, and the width is 50–200 nm, while the length can be as high as several tens of micrometers, or even millimeters. The morphologies undergo no obvious changes through the phase transformation process from $Na_2Ti_3O_7$ to $H_2Ti_3O_7$ to TiO_2 NBs as long as the reaction procedures are controlled carefully.

As illustrated in Fig. 1b, the formation process of TiO_2 NBs includes three primary stages that are shown in the three equations that follow. First, the TiO_2 precursor is dissolved by breaking the Ti-O-Ti bonds, causing the formation of $Na_2Ti_3O_7$ NBs. Second, the $Na_2Ti_3O_7$ NB is converted to $H_2Ti_3O_7$ NB by the ion-exchange process. Finally, the $H_2Ti_3O_7$ NB is annealed to produce TiO_2 NBs through a process of dehydration and crystal-lattice rearrangement.

$$3TiO_2 + 2NaOH \rightarrow Na_2Ti_3O_7 + H_2O \qquad (R1)$$

$$Na_2Ti_3O_7 + 2HCl \rightarrow H_2Ti_3O_7 + 2NaCl \qquad (R2)$$

$$H_2Ti_3O_7 \rightarrow 3TiO_2 + H_2O [40] \qquad (R3)$$

The key point for the generation of the belt-like morphology is the formation of sodium titanate NBs, and the formation mechanism of such titanate NBs has been widely investigated [49,50].

The hydrothermal method is actually a time-consuming process because it requires three main steps: hydrothermal synthesis, acid treatment, and calcination. Due to its attractive advantages, such as the potential for mass production, low cost, and controllable ribbon-like morphology, it is still the most popular method
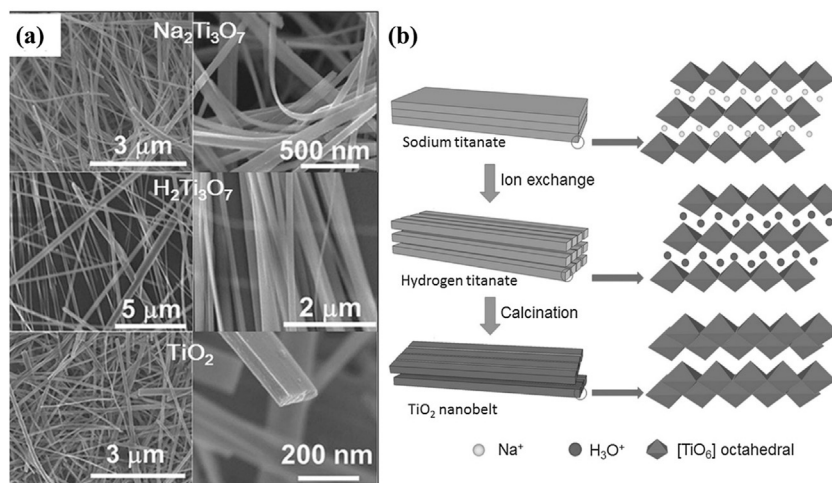
Fig. 1. (a) Typical SEM images of $Na_2Ti_3O_7$, $H_2Ti_3O_7$ and TiO_2 NBs. Reproduced with permission [48] Copyright 2008, WILEY-VCH Verlag GmbH & Co. KGaA, Weinheim; (b) Schematic illustration of the formation mechanism of TiO_2 NBs. The $[TiO_6]$ octahedral consists of one Ti atom and six O atoms, with the Ti atom in the center and the six O atoms in the corners of the octahedral [40] Copyright 2015, WILEY-VCH Verlag GmbH & Co. KGaA, Weinheim.

carried out in most studies related to TiO_2 NB. Recently, we have realized the kilogram-level production of TiO_2 NB by using a 60 L stainless steel autoclave by the modified hydrothermal method. This pilot production (1.1 kg of production) was proceeded in our cooperative company, Jiaxing Rejdue Environmental Technology Co., Ltd.

2.1.2. Solvothermal methods

The solvothermal method is very similar to the hydrothermal method except that organic liquid chemicals that are free of water are used as the solvent in the reaction system [51]. The solvothermal method has become a favored method to synthesize TiO_2 nanostructures because of its superior control of the size distributions and the uniform morphology and high crystallinity of the resulting TiO_2 nanostructures compared with the hydrothermal method [52]. In addition, the solvothermal method has proved to be a versatile technique for synthesizing various TiO_2 nanoparticles with a narrow size distribution and good dispersity by using different organic Ti compounds, such as titanium chloride ($TiCl_4$) [53], titanium butoxide ($Ti(OBu)_4$) [54], and $TiOSO_4$ [55] as the titanium sources. Compared with alkali-hydroxide hydrothermal method, the most important characteristic of this method is that TiO_2 NBs can be obtained in a one-step process without any additional treatment [56,57]. More importantly, biphasic ultrafine TiO_2 NBs with coexisting anatase and rutile phases can be obtained directly through this one-step reaction, and the size of the TiO_2 NBs are much smaller than those obtained from the hydrothermal method.

Typically, using *N,N*-dimethylformamide (DMF) and acetic acid (HAc) with a certain volume ratio as the organic solvent and titanium (IV) butoxide (TB) as the Ti precursor, biphasic ultrafine TiO_2 NBs can be obtained via a solvothermal process at 200 °C for 20 h. Compared with TiO_2 NBs synthesized by solvothermal methods, besides the smaller size, the biphasic ultrafine TiO_2 NBs have a larger specific area and more active facets, which would lead to an improved photocatalytic activity.

2.1.3. H_2O_2-assisted wet chemistry methods

Another attractive method is the alkaline-free H_2O_2-assisted wet chemistry route at ambient conditions reported by Wu et al. (Fig. 2) [58–60]. Glycine, titanium oxysulfate-sulfuric acid hydrate and nitric acid are used to prepare the Ti precursor, then the precursor reacts with H_2O_2 at room temperature to obtain the titanate

ultrafine NBs. Well-crystallized anatase ultrafine TiO_2 NBs are produced after calcination at 400 °C.

The as-prepared ultrafine titanate NBs have a leaf-like shape with very small thickness of approximately 1 nm. Compared with hydrothermal methods, this method is energy efficient and proceeds to get titanate without heating or external thermal/mechanical activation. Moreover, the obtained ultrafine TiO_2 NBs have a smaller thickness and larger specific area, which causes high photocatalytic activity.

2.2. Structural characteristics of TiO_2 NBs

As mentioned above, the morphology of the NBs depends on the synthesis method. The evolution of crystallization and the morphologies of the TiO_2 NBs synthesized by a typical alkaline hydrothermal procedure are illustrated in Fig. 3. As reported by Wang et al. [48], TiO_2 NBs synthesized by the hydrothermal-based approach possess a well-defined belt-like structure, normally 20–40 nm thick, 50–200 nm wide and with a length that usually varies from several micrometers to the millimeter range [62]. The crystalline structure of anatase TiO_2 NBs can be assigned to a tetragonal anatase phase with the following lattice parameters: a = b = 0.3766 nm and c = 0.9486 nm based on XRD and Raman results. From the selected area electron diffraction (SAED) patterns of a single anatase TiO_2 NB, the crystal grows along the [101] direction with two dominant (101) facets exposed, and the top facet is confirmed to be the (001) facet [11].

Ultrafine TiO_2 NBs can be obtained by a solvothermal method [57]. As observed from Fig. 4, the thickness of the ultrafine NBs is smaller than 5 nm, while the width is 10–20 nm, and the length is over 100 nm. They grow in the [101] direction with the (010) facet exposed. The ultrafine NBs are composed of two phases, rutile and anatase, which is beneficial for photocatalysis because of the band gap matching effect between these two semiconductors. By tuning the synthesis conditions, the morphology and phase composition of the NBs can be controlled [57].

Fig. 5 shows the crystal structure and the morphologies of ultrafine TiO_2 NBs synthesized by H_2O_2-assisted wet chemistry methods. The crystal is assigned as anatase based on the XRD and Raman results. The thickness is larger than that of the as-synthesized titanate but no more than 5 nm, which can be attributed to phase transition and grain growth during the calcination process. The interplanar space of 0.35 nm corresponds to the (101) spacing of anatase.
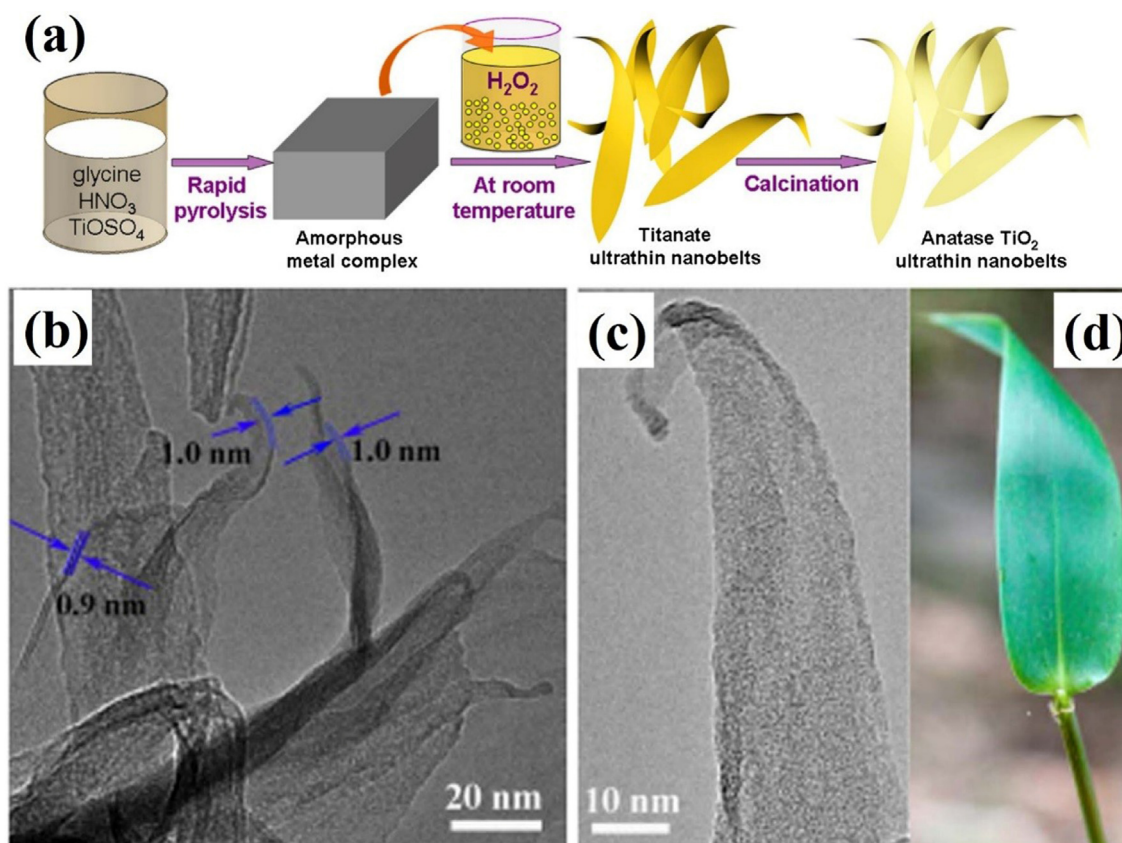
Fig. 2. (a) A schematic illustration showing the novel synthesis procedure of anatase ultrafine TiO₂ NBs. (b) TEM and (c) HRTEM images of as-prepared ultrafine titanate NBs and (d) an optical photograph of a bamboo leaf [58] Copyright 2016, Macmillan Publishers Limited, part of Springer Nature.

Fig. 3. (a) Bright-field TEM image of an anatase NB and the selected area electron diffraction pattern taken along the [100] direction; (b) HRTEM image [61] Copyright 2010, American Chemical Society.

2.3. Basic properties of TiO₂ NBs

As one of the most attractive semiconductor photocatalysts, TiO₂ NB has several advantages, which means TiO₂ NBs have var-ious potential applications [49]. TiO₂ NBs have a high chemical stability; they are resistant to weak acids as well as weak bases and insoluble in water. Most importantly, the belt-like structure of TiO₂ NBs has brought about some desirable advantages as a promis-

Fig. 4. Ultrafine TiO$_2$ NBs synthesized by a solvothermal method. (a) SEM image, (b)–(d) TEM and HRTEM images, and (e) XRD pattern of the NBs [57] Copyright 2016, The Royal Society of Chemistry.

Fig. 5. NBs synthesized by a H$_2$O$_2$-assisted wet chemistry method. (a) XRD pattern. (b) Raman spectrum, (c) SEM, (d)–(e) TEM, and (f) HRTEM images (inset: SAED pattern). (g) Nitrogen adsorption-desorption isotherm (inset: pore size distribution) of as-prepared anatase ultrafine TiO$_2$ NBs [58] Copyright 2016, Macmillan Publishers Limited, part of Springer Nature.

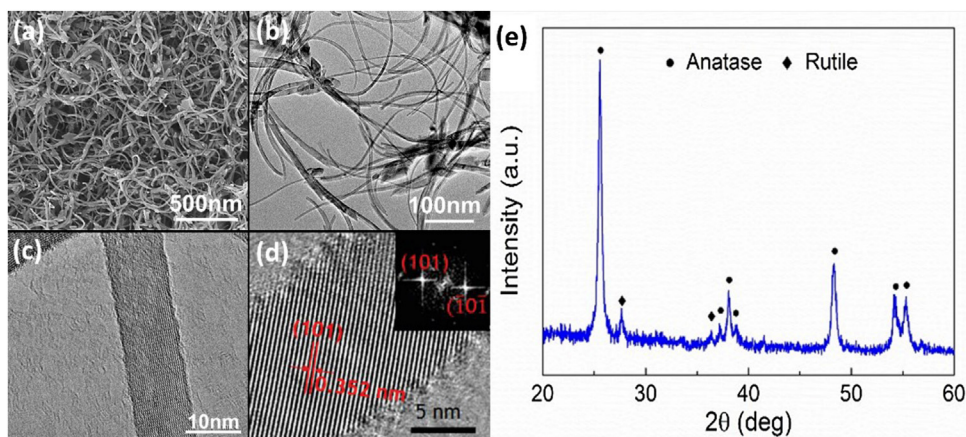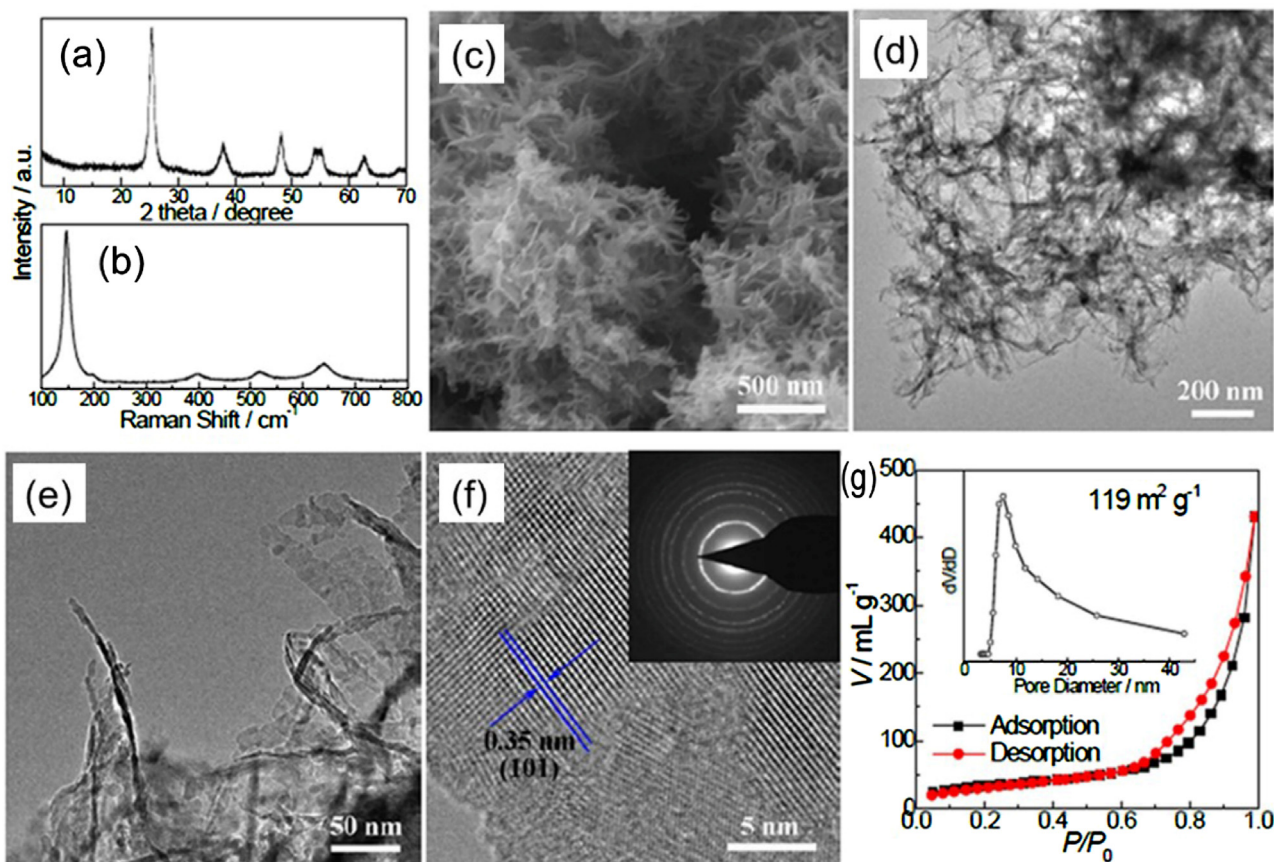ing photocatalyst. Firstly, because the thickness of the TiO$_2$ NBs is smaller than the electron mean-free path, with the high crystallinity of the single anatase phase, a carrier in the TiO$_2$ NBs can be transferred with a high speed, which is beneficial for photo-induced carrier transfer and effective separation [11]. Secondly, the typical one-dimensional structure, which provides a large length-to-diameter ratio and good flexibility, makes it possible for the NBs to be used in recycling applications and enables the fabrication of nanopaper that can be used in continuous filtration photocatalysis. Thirdly, the relative large surface area makes it a desired

building block for the assembly of various nanostructures to form heterostructures with enhanced properties without losing the high UV photocatalytic property of the TiO$_2$ substrate. However, TiO$_2$ NBs still have some negative characteristics with regards to their use in photocatalysis. Similar to other TiO$_2$ nanostructures, TiO$_2$ NBs have a large band gap (>3.0 eV) [63], which leads to the limited light response that occurs only within ultraviolet region. Visible and infrared light cannot be absorbed, which is a significant obstacle to the use of solar light as the light resource for photocatalysis. Furthermore, TiO$_2$ NBs produced by the hydrothermal method are

usually single-phase materials, and this is adverse to the separation of photo-induced carriers. In addition, the primary exposed facet of TiO₂ NBs, the (101) facet, has a very low photocatalytic activity, resulting in an undesirable performance from the NBs [48].

On the basis of the above characteristics of TiO₂ NBs, we have proposed a method of constructing surface heterostructures on TiO₂ NBs to construct high-performance hybrid photocatalysts, TiO₂ NSHs, which not only fully use the advantages of TiO₂ NBs but also completely overcome their other shortcomings. In this way, the well-designed TiO₂ NSHs should have the following characteristics: (1) enhanced light harvesting and more active sites; (2) broader light absorption from UV to visible light and even near-infrared light; (3) improved ability to separate photo-generated carriers, leading to high-performance photocatalysts [11]. Therefore, TiO₂ NB heterostructures can be used as a powerful tool to build high-performance photocatalysts. Therefore, a clear understanding of the basic theory of photocatalytic reactions and the design principle for high-performance TiO₂ NB heterostructures for photocatalysis becomes an important prerequisite for their synthesis and applications.

3. Mechanisms of the photocatalysis process and design principles for TiO₂ NB heterostructures

Photocatalytic performance is mainly determined by the intrinsic energy band structure of the photocatalysts. The energy band structure can intensively influence the energy-level transitions and the transport of electrons, which depend on the composition, valence of atoms, and crystal structure of the photocatalysts [64]. The light absorption, redox potential, charge-carrier mobility, and consequent photoactivity of the semiconductors can be adjusted by modifying the band structure [65]. To obtain photocatalysts with more favorable properties, the mechanism of photocatalysis and the design principle for photocatalysts should first be clearly understood.

3.1. Mechanism of photocatalysis

Although the mechanism of photocatalysis can be found in almost all the reviews about photocatalysts, we prefer to give a brief introduction of this mechanism because it is integral to this review and helps us better understand the design of TiO₂ NB surface heterostructures. Photocatalysis is a photoreaction process that is accelerated by a catalyst, and almost all photocatalysts are semiconductors [66]. All semiconductors have an intrinsic valence band and conduction band, which determine the bandgap. When light with a fixed wavelength is irradiated on the semiconductor, if the photon energy of the light is higher than or equal to the width of the semiconductor bandgap, the photon is captured. The electrons (e⁻) gain enough energy to move from the valence band to the conduction band, and a corresponding hole (h⁺) is formed in the valence band; this is referred to as an electronic transition. Next, the electrons and holes separate in different directions, but simultaneously, a number of the charge carriers (electron-hole pairs) recombine. When electrons and holes reach the surface of photocatalysts, the strong oxidation-reduction ability can drive many types of redox reactions, such as water splitting for hydrogen generation and degradation of organic pollutants in wastewater.

Therefore, the photocatalytic process, which is shown in Fig. 6, can be roughly divided into the following steps: 1) light harvesting and absorption; 2) electronic transition and the formation of charge carriers (electron-hole pairs); 3) separation of electron-hole pairs and movement of electron-hole pairs to the photocatalyst surface; 4) participation of electrons and holes in redox reactions on the surface. To improve the photocatalytic efficiency, we must strengthen
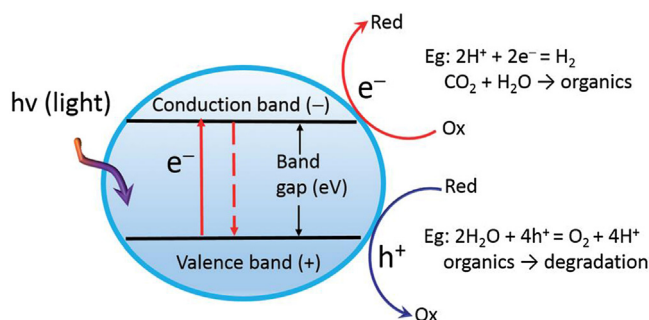

Fig. 6. A schematic illustration of the photocatalysis process [64] Copyright 2015, WILEY-VCH Verlag GmbH & Co. KGaA, Weinheim.

all these steps in the photocatalysis process. Therefore, the design principles of TiO₂ NSH photocatalysts can be determined based on this process; these principles are stated in the next section.

3.2. Design principles of TiO₂ NSHs photocatalysts

The photocatalysis process is mainly determined by the four steps mentioned above. These steps are closely related to the properties of the photocatalysts. Therefore, we must try to strengthen every step of the photocatalytic process to obtain high-performance photocatalysts. Through this, we can infer the basic principles of designing TiO₂ NB surface heterostructured photocatalysts: 1) to enlarge the photocatalytically active surface, 2) to strengthen and broaden light absorption, and 3) to promote the separation of charge carriers. The aim of designing TiO₂ NSHs is to overcome the shortcomings of pure TiO₂ NBs and improve their photocatalytic activity. By following these principles, we have designed and prepared many types of TiO₂ NSHs with excellent photocatalytic performance.

3.2.1. Enlargement of the photocatalytically active surface

The photocatalytic reaction process mainly occurs on the surface of photocatalysts, thus the enhanced photocatalytic efficiency can be realized by enlarging the active photocatalytic surface. Normally, there are two effective ways of achieving this. The first one is to enlarge the specific surface area of the photocatalysts. The second is to increase the activity of the photocatalyst surface, in other words to increase the exposure of the active sites [67–69].

Enlargement of the specific surface area. It is clear that catalysts with a smaller size have a larger specific surface area. However, it is difficult to separate photocatalysts with an extremely small size from the reaction system after the reaction, which results in a high recycling cost or secondary pollution. Therefore, P25 is not an ideal photocatalyst for industrial applications. For TiO₂ NBs with a particular size and morphology, an effective method of enlarging the specific surface area is by increasing the roughness of the surface of the NBs, such as by creating bumps or dents. In addition, synthesizing TiO₂ NBs with a smaller size, or smaller thickness, is another important way of enlarging the surface area of TiO₂ NBs, and this enlargement may also enhance the photocatalytic properties. However, the exposed facet of TiO₂ NBs is more important for photocatalytic activity than their specific surface area.

Obtaining more photocatalytically active facets. As is well known, although TiO₂ has perfect UV light photocatalytic performance, not all facets of the TiO₂ crystal have the same photocatalytic activity. For anatase TiO₂, the order of the surface energy of the different facets is (001) > (100) > (101), and the photocatalytic activity of the different facets is dominated by the surface energy [70]. Therefore, it is important to expose as much as possible of the crystal facets with higher photocatalytic; these are also the facets in which photocatalytically active sites are most densely
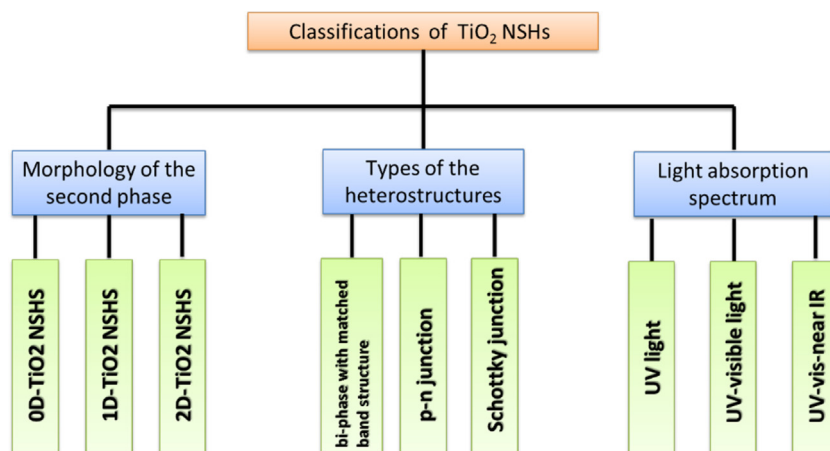
Fig. 7. Classification of TiO$_2$ NSHs.

distributed. For TiO$_2$ NBs, the growth direction can be tuned by using special capping agents [61], but a more facile and practical method for obtaining more active photocatalytic facets is the acid-etching process [71]. In addition, assembling well-distributed second-phase nanoparticles with a large number of active facets is a very important approach for building high-performance TiO$_2$ NB-based photocatalysts. Our group has made significant effort in this area, and the results from this research will be introduced in detail in Section 4.

3.2.2. Enhancement of light absorption and broadening of the photocatalytically active light band

For photocatalysis, there are several different ways to enhance and broaden the light absorption. Enhancing light absorption means capturing as much photon energy as possible, and transferring the photons into electron-hole pairs. As mentioned above, most of the solar energy is distributed in the visible and infrared light regions, and UV light accounts for only 4% of the total solar energy. However, due to the intrinsic band structure of TiO$_2$, only UV light ($\lambda < 380$ nm) can achieve photoelectric conversion, so most of the solar energy is not utilized efficiently. Therefore, even if all the UV light from sunlight is absorbed by TiO$_2$ for photocatalysis, the available solar energy will be no higher than 4% of the total energy. Therefore, the light absorption rate of the TiO$_2$ nanostructures is still limited without a broadened absorption band. Based on this, broadening the light absorption range of TiO$_2$ NBs from the UV to the visible and near-infrared regions is important for building TiO$_2$ NB-based high-performance photocatalysts.

The most popular method of endowing TiO$_2$ NBs with visible and/or infrared light photocatalytic activity is by assembling a second phase on the surface of the NBs to form TiO$_2$ NSHs. There are various reaction mechanisms in different TiO$_2$ NSHs that determine how the introduction of the second phase can broaden the light absorption spectrum of TiO$_2$ NSHs photocatalysts. For example, some of the second phase components have visible or infrared light photocatalytic activity themselves, while others have an up-conversion function or plasmonic effects that enhance the light absorption property. Some examples of building TiO$_2$ NSHs photocatalysts to realize high-performance photocatalysts with broadened light absorption for photocatalytic activity will be provided in Section 4 and 5.

3.2.3. Promoting the separation of the photo-induced charge carriers

As mentioned above, charge carriers (electron-hole pairs) can be formed in TiO$_2$ nanostructures through photoelectric conversion when the nanostructures absorb photons during the photocatalysis process. If the photo-induced electrons and holes cannot move directionally to the surface to participate in the photocatalytic reaction, they will quickly recombine in situ, release energy in the form of light or heat, and lose their photocatalytic function. Therefore, suppressing the recombination of charge carriers is one of the key factors in improving the photocatalytic efficiency. TiO$_2$ NBs, due to their dimensional limitations, can induce some charge carriers to move directionally to the surface of the photocatalysts, but a number of them will also recombine before reaching the surface because of the single-crystalline structure. To promote the separation of the photo-induced charge carriers, nanoparticles with a second phase can be synthesized on surface of the TiO$_2$ NBs to form TiO$_2$ NSHs based on different physical mechanisms. The mechanisms and categories of heterostructures used to promote the separation of carriers are borrowed from semiconductor technology, in which heterojunctions built by two types of semiconductors or a semiconductor and metal can tune the interface band structure and cause the directional transport of carriers. The design principle of heterojunctions has been widely used in electronic devices, including *p-n* junctions, Schottky junctions and band matching structures, which have been used to build high-performance TiO$_2$ NSH photocatalysts. Some examples that use the above principles will be introduced in Section 4.

4. Synthesis, photocatalytic performance and applications of TiO$_2$ NSHs

To date, TiO$_2$ NSHs with different properties have been designed and synthesized for several different applications. In this review, we mainly focus on the TiO$_2$ NSHs for photocatalysis applications. There are several classification methods to categorize TiO$_2$ NSHs according to different characteristics of the nanostructures (Fig. 7). According to the morphology of the second phase loaded on the NBs, they can be divided into 0D/1D/2D-TiO$_2$ NSHs, which correspond to nanoparticles, nanorods and nanosheets, respectively. According to the type of the heterojunction formed by the tuning effect of the interface band structure, these NSHs can be divided into single component heterostructures, *p-n* junctions, Schottky junctions and bi-phase junctions with matched band structures. In addition, they can also be classified by the light absorption range in the photocatalytic reaction, such as UV–vis photocatalysts and UV-vis-IR light photocatalysts. In recent years, Z-scheme heterostructure was proposed and many photocatalysts based on Z-scheme exhibited enhanced photocatalytic activity [72]. However, there are no Z-scheme photocatalysts based on TiO$_2$ NBs, so

this field contains huge potential. In this section, we would like to introduce the synthesis methods, structures, photocatalytic performance and some of the mechanisms of TiO_2 NSHs based on the types of heterojunction.

Although photocatalysis has several different applications, photodegradation of organic pollutants [73] and photocatalytic water splitting for hydrogen generation [74] are two of the most popular applications. It is well known that the capabilities of organic degradation and water splitting demand different photocatalyst characteristics. The photocatalysts with a higher over-potential are more beneficial to water splitting for hydrogen generation [75], while organic degradation, which follows a capture-degradation-release process [76], needs catalysts that have a strong affinity for absorbing specific organic matter [77].

Most TiO_2 NSHs are prepared through wet-chemical approaches by using common as-synthesized TiO_2 NBs, such as the surface-coarsened TiO_2 NBs (C-TiO_2 NBs, which are also called the TiO_2-nanoparticle/TiO_2-NB surface heterostructures or TiO_2-P/TiO_2-B NSHs) [71] or the double-crystalline phase heterostructured TiO_2 NBs as substrates [62]. These TiO_2 NSH photocatalysts exhibit excellent performance and are favored in the development of scientific research and practical photocatalysis applications.

4.1. Single-component TiO_2 NSHs

Single-component TiO_2 NSHs refer to heterostructures where the two parts of the heterostructure are TiO_2 with different phases or different morphologies. Based on the morphology and phase compositions of TiO_2 NSHs, single-component TiO_2 NSHs can be divided into three categories: single-phase compositions with two morphologies, such as TiO_2-P/TiO_2-B NSHs [71], single morphology NSHs with two phase compositions, such as TiO_2(B)/anatase TiO_2 core-shell NB heterostructures [62] and TiO_2 NSHs with different morphologies and different phase compositions. The following section provides a brief introduction of the synthesis and photocatalytic properties of TiO_2-P/TiO_2-B NSHs and TiO_2(B)/anatase TiO_2 core-shell NB heterostructures.

4.1.1. TiO_2-P/TiO_2-B NSHs and their photocatalytic properties

As mentioned above, TiO_2 NBs possess low photocatalytic activity because most of the exposed facets on their surface are low-energy facets. Granular TiO_2 particles have a large surface area, and almost all the different facets of the crystal can be found on the surface of the particles. Therefore, by assembling a large number of TiO_2 granular nanoparticles on TiO_2 NBs to form TiO_2-P/TiO_2-B heterostructures, the photocatalytic property can be improved. Moreover, as reported previously, photo-induced carrier separation can occur between two different facets of TiO_2 [78], which can further enhance the photocatalytic performance of TiO_2 NBs.

The Liu group has developed a facile method of constructing TiO_2-P/TiO_2-B NSHs based on an acid-assisted hydrothermal method [71]. The detailed hydrothermal-based process for the synthesis of TiO_2-P/TiO_2-B NSHs is shown in Fig. 9. As mentioned above, $H_2Ti_3O_7$ NBs are obtained directly by immersing $Na_2Ti_3O_7$ NBs in HCl solution. TiO_2-P/TiO_2-B NSHs are synthesized from $H_2Ti_3O_7$ NBs. Briefly, $H_2Ti_3O_7$ NBs are mixed with 0.02 M H_2SO_4 aqueous solution under ultrasonic irradiation for 10 min. The mixed suspension is transferred into a Teflon-lined stainless steel autoclave and heated at 100 °C for 6–24 h. The powder product was then thoroughly washed with distilled water and dried in a drying cabinet. The dried powder was calcined at 400–1000 °C for 2 h to obtain TiO_2-P/TiO_2-B NSHs. The SEM and TEM images of the samples are shown in Fig. 8.

It can be observed from Fig. 8 that TiO_2 nanoparticles grow on the surface of the TiO_2 NBs, and the lattices of both sides connect together to form typical heterojunction structures. Although

both the substrate and nanoparticle have the same composition and crystal phase, the high photocatalytic property of the nanoparticles and the high carrier transport property of the NBs endow the TiO_2-P/TiO_2-B NSHs high photocatalytic properties. The acid concentration, acid treatment time, hydrothermal treatment time, and heat treatment time are the key parameters for building high-performance TiO_2-P/TiO_2-B NSHs [71]. As shown in Fig. 9, the acid treatment time and thermal treatment temperature can tune the phase composition and thereby affect the photocatalytic property of TiO_2-P/TiO_2-B NSHs. The optimized acid treatment conditions involve immersing the $H_2Ti_3O_7$ NBs in H_2SO_4 solution for 24 h and then calcining them at 600 °C for 2 h.

Another example of single-component TiO_2 NB heterostructures is the anatase TiO_2/nanoparticle TiO_2-B NB heterostructure synthesized by a layer-by-layer assembly method [79]. The photoelectric conversion efficiency of the heterostructures proved to be much higher than that of single-phase TiO_2 NBs.

4.1.2. TiO_2(B)/anatase interface NB heterostructures

In addition to TiO_2-P/TiO_2-B NSHs, biphasic TiO_2 NBs are another type of single-component TiO_2 NB heterostructures [62]. The band matching between two phases that coexist in the same TiO_2 NB can promote the photo-induced carrier separation, and thus the photocatalytic activity of TiO_2 NBs can be improved. Based on this principle, some studies related to biphasic TiO_2 NB heterostructures have been reported. Fujishima et al. reported that novel TiO_2 heterogeneous nanostructures, in which anatase nanoparticles were assembled on rutile nanorods, showed improved photocatalytic activity [80]. Li et al. synthesized anatase/TiO_2(B) core-shell NBs from potassium titanate $K_2Ti_5O_{11}$ through an alkali-hydrothermal method that followed ion exchange and calcination [81]. The core-shell NBs possessed a high photocatalytic property. Yang et al. have also synthesized TiO_2(B)/anatase core-shell NBs by selectively doping cerium ions into the TiO_2(B) core. It was verified that the photocatalytic property was enhanced by doping the heterostructure [82].

To illustrate the synthesis of two-phase TiO_2 core-shell heterostructures and their enhanced photocatalytic property, we use TiO_2(B)/anatase interface NB heterostructures synthesized by Zhou et al. [62] as an example. As was mentioned in Section 2, TiO_2 NBs can be synthesized through a three-step process: $Na_2Ti_3O_7$ NBs are synthesized by an alkali-hydrothermal process, $Na_2Ti_3O_7$ NBs are transformed to $H_2Ti_3O_7$ NBs by an ion-substitution process, and $H_2Ti_3O_7$ NBs are decomposed to form TiO_2 NBs by a heat-treatment process. During the heat treatment process, $H_2Ti_3O_7$ loses the water it contains and is first transformed to TiO_2(B); then it transforms to anatase and finally rutile NBs with an increase in the treatment temperature. With an increasing heat-treatment temperature and a low heating speed, the constituent water in the $H_2Ti_3O_7$ NBs is totally removed, and a low-temperature phase, TiO_2(B), forms first. Upon increasing the heating temperature further, the outermost layer transforms to anatase, and grows toward to the center part of the TiO_2(B) NB. By carefully controlling the heating speed, heating temperature, and soaking time, a TiO_2(B)/anatase core-shell NB heterostructure can be obtained. This heterostructure possesses an enhanced photocatalytic ability compared with pure TiO_2(B) and anatase NBs. The band edges of the two phases are matched to guide photo-induced electrons towards the TiO_2(B) core, and the photo-induced holes migrate to the anatase shell, which causes an increased photo-induced carrier separation and enhances the photocatalytic activity.

As shown in Fig. 10, the TiO_2(B)/anatase core-shell NB heterostructures obtained at 800 °C have the best photocatalytic activity, with a MO degradation ratio of 100% in 50 min, which is superior to that of the pure TiO_2(B) NBs (obtained at 400 °C) and
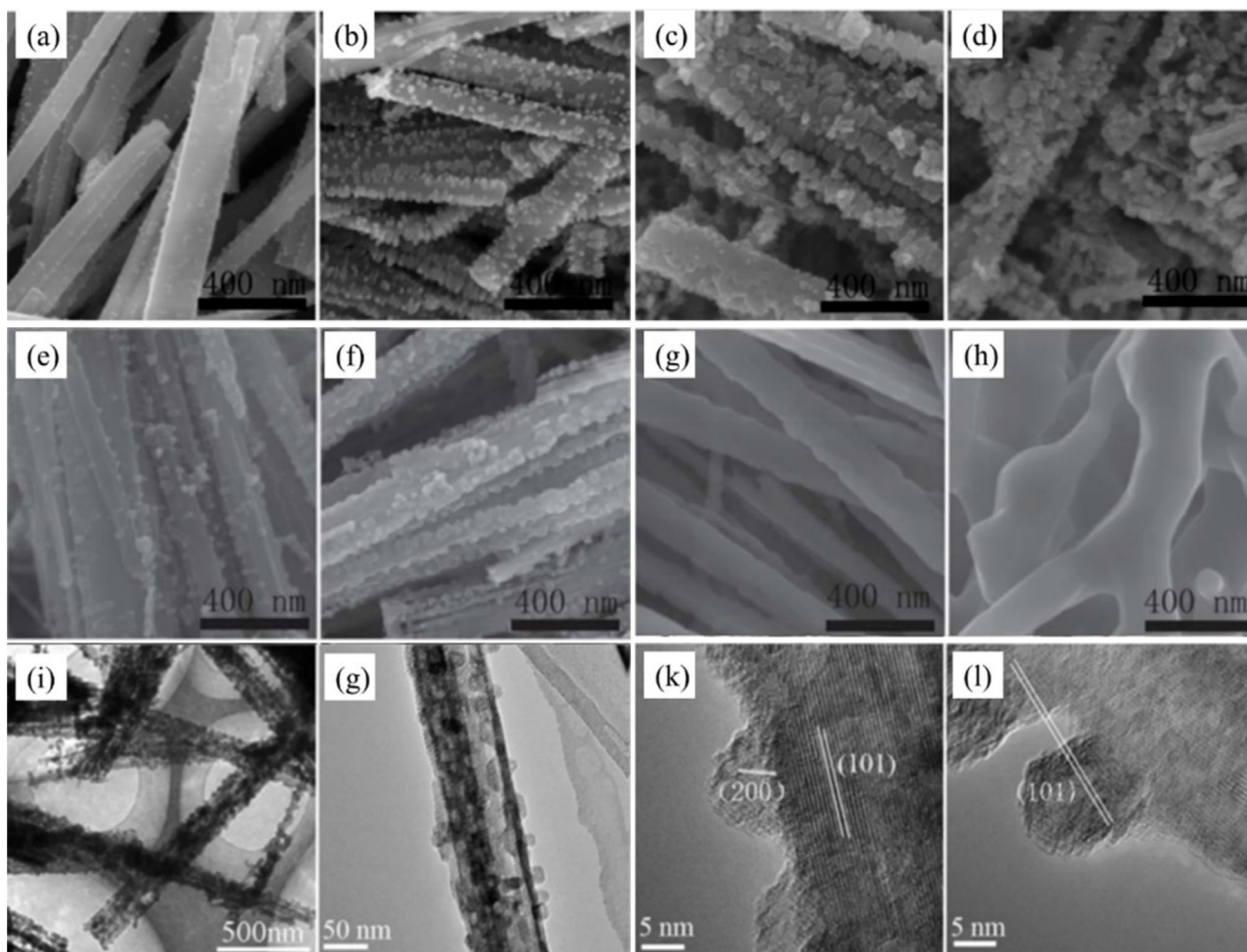
Fig. 8. (a)–(d) SEM images of $H_2Ti_3O_7$ NBs with different acid treatment times, (a) 6 h, (b) 12 h, (c) 24 h, (d) 36 h; (e)–(h) SEM images of TiO_2-P/TiO_2-B with different calcination temperatures, (e) 400 °C, (f) 600 °C, (g) 800 °C, (h) 1000 °C; (i)–(l) TEM and HRTEM images of TiO_2-P/TiO_2-B NSHs at different magnifications [71] Copyright 2011, The Royal Society of Chemistry.

anatase NBs (obtained at 900 °C), whose degradation ratios are 40% and 73%, respectively.

As stated above, TiO_2-P/TiO_2-B and TiO_2(B)/anatase interface heterostructure NBs show superior performance compared with common TiO_2 NBs because of their higher number of active sites and more effective photo-induced carrier separation. However, because the enhancement of photocatalytic performance of these types of TiO_2 NB heterostructures is limited, other TiO_2 NSHs based on semiconductor mechanisms, such as *p-n* junctions, Schottky junctions, plasmonic enhancement, and the assembly of visible and near-infrared light photocatalytically active nanoparticles on TiO_2 NBs have been proposed and synthesized.

4.2. TiO₂ NSHs with p-n junctions

A *p-n* junction is a space-charge region normally formed by joining a p-type and n-type semiconductor together in very close contact [83]. The construction of *p-n* junctions with a built-in electric field between two semiconductor photocatalysts is an efficient approach to separate photo-induced charge carriers and enhance photocatalytic activity [84].

4.2.1. The formation of p-n junctions and a built-in electric field

The electrical conductivity of n-type semiconductors is mostly derived from free electrons due to their high free electron concentration, while p-type semiconductors possess a high concentration of "holes" (the equivalent of positive charge), which become the main conductive carriers. Holes in n-type semiconductors and electrons in p-type semiconductors are almost negligible.

Due to the concentration difference of free electrons and holes between the two parts of a *p-n* junction, electrons tend to diffuse from the n-type region to the p-type region; at the same time, holes tend to move in the opposite direction. As a result, the p-area loses holes, leaving negatively charged ions, while the n-area loses electrons, leaving positively charged ions. These charged particles cannot move freely in the vicinity of the interface, so they form a built-in electric field [85–87]. This process is demonstrated in Fig. 11.

4.2.2. Enhancement of photocatalytic efficiency by p-n junctions and the built-in electric field effect to promote the separation of charge carriers

In Fig. 11, it is obvious that the direction of the built-in electric field is opposite to the direction of diffusion of the charge carriers. When light with a certain wavelength is absorbed by the photocatalysts, many electron-hole pairs will be formed due to the photoelectric conversion that occurs during the photocatalytic process. The newly formed charge carriers will move along the direction of the electric field force. Holes will move to the p-type region and electrons will move to the n-type region. From another point of view, the directions the electrons and holes move towards fundamentally depend on the specific band structures of the two
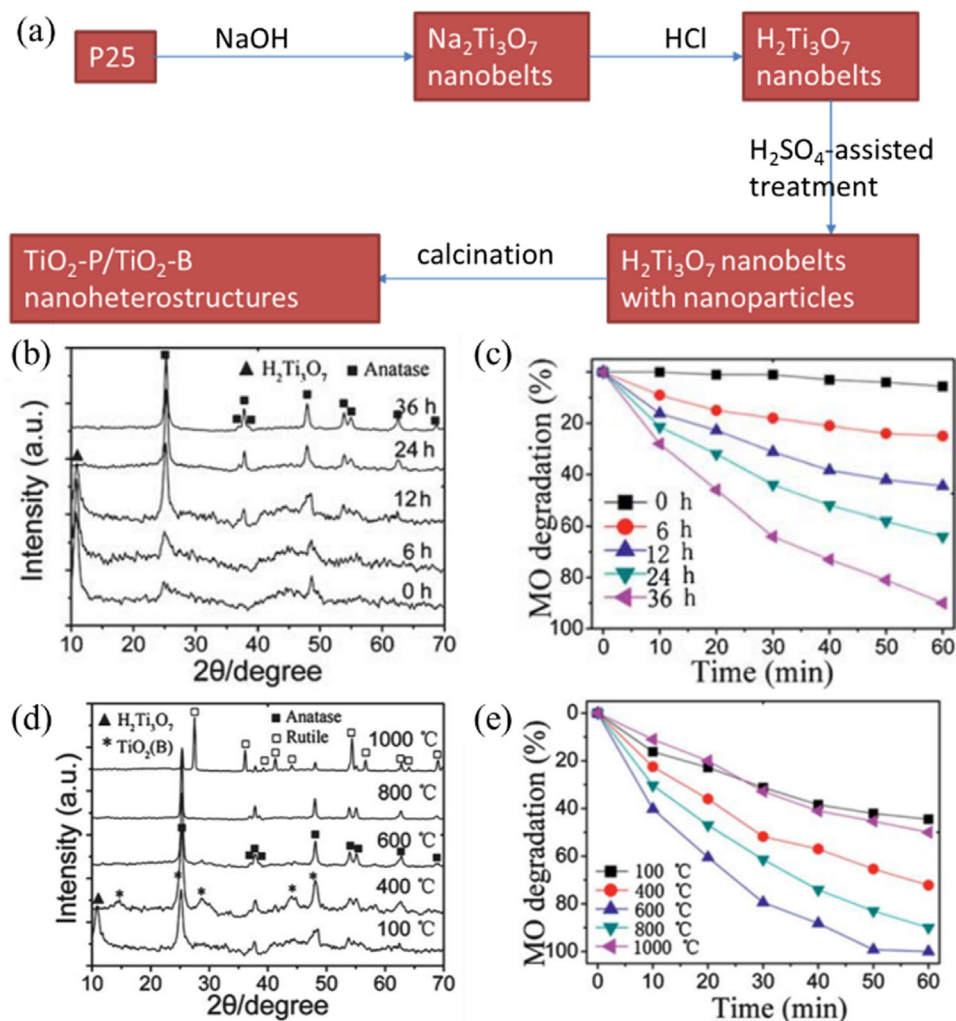
Fig. 9. (a) Synthesis process of TiO$_2$-P/TiO$_2$-B; (b) XRD patterns and (c) UV photocatalytic activity of the as-synthesized H$_2$Ti$_3$O$_7$ NBs with different acid corrosion times; (d) XRD and (e) UV photocatalytic activity of the as-synthesized TiO$_2$-P/TiO$_2$-B heterostructures obtained with different temperatures: (a) 400, (b) 600, (c) 800 and (d) 1000 °C [71] Copyright 2011, The Royal Society of Chemistry.

types of semiconductors. In one word, the *p-n* junction and built-in electron field effect promote the separation of electron-hole pairs. When electrons and holes reach the surface, they are consumed in the redox reaction; new photo-induced carriers continue to separate and photocatalysis can proceed continuously.

It is well known that TiO$_2$ is an intrinsic n-type semiconductor because of the presence of an O vacancy [88]. If it were assembled with a p-type semiconductor nanostructure with photocatalytic properties to form *p-n* junctions, theoretically, the assembly would significantly enhance the separation of charge carriers and improve the photocatalytic efficiency. Unfortunately, most of the oxide semiconductors are n-type because of the vacancy of O atoms, while p-type semiconductors are relatively scarce.

Based on the *p-n* junction theory described above, several types of TiO$_2$ NSHs with *p-n* junctions have been prepared, which exhibit high photocatalytic efficiency. Yang et al. synthesized a unique Cu$_2$O/TiO$_2$ *p-n* heterojunction network catalyst with a highly efficient photocatalytic degradation of p-nitrophenol [89]. NiO is an ideal p-type semiconductor used with TiO$_2$ NBs. Chen et al. obtained a *p-n* junction NiO/TiO$_2$ photocatalyst by a sol-gel method [90]. Dai et al. prepared *p-n* junction BiOI/TiO$_2$ nanotube arrays with enhanced visible-light photoelectrocatalytic activity [91]. There are four types of heterojunctions (namely p-p, *p-n*, n-n, n-p) according to the band structure relationship between the two parts of

the heterostructure, among which the type-II *p-n* junction is the ideal heterojunction [92]. TiO$_2$ can be assembled with different types of semiconductors to form different types of *p-n* junctions. Sarkar et al. synthesized three-dimensional Ag$_2$O/TiO$_2$ type-II (*p-n*) nanoheterojunctions, which show superior photocatalytic activity [93].

4.2.3. NiO/TiO$_2$ NSHs with p-n junctions

Among the numerous types of metal oxide, NiO is an ideal p-type semiconductor used to form *p-n* junctions with TiO$_2$ due to its band structure, good performance and low cost [94]. Therefore, NiO/TiO$_2$ nano-*p-n* junction structures have been intensively researched and several types of NiO/TiO$_2$ *p-n* junction nanostructures have been synthesized through different methods.

Lin et al. synthesized nano-*p-n* junction TiO$_2$ NSHs by assembling p-type semiconductor NiO nanoparticles on the surfaces of n-type TiO$_2$ NBs [83] to enhance the photocatalytic properties of TiO$_2$ NBs. The pure TiO$_2$ NBs and C-TiO$_2$ NBs are used as the substrate. Here, we use the synthesis of NiO nanoparticle(-NP)/TiO$_2$ NSHs as an example to demonstrate the synthesis of *p-n* TiO$_2$ NSHs.

Pristine H$_2$Ti$_3$O$_7$ NBs were prepared through a hydrothermal method, and C-H$_2$Ti$_3$O$_7$ NBs need an additional acid-assistant corrosion process, which was introduced before. NiO nanoparticles can be loaded through a chemical-solution-deposition-decomposition
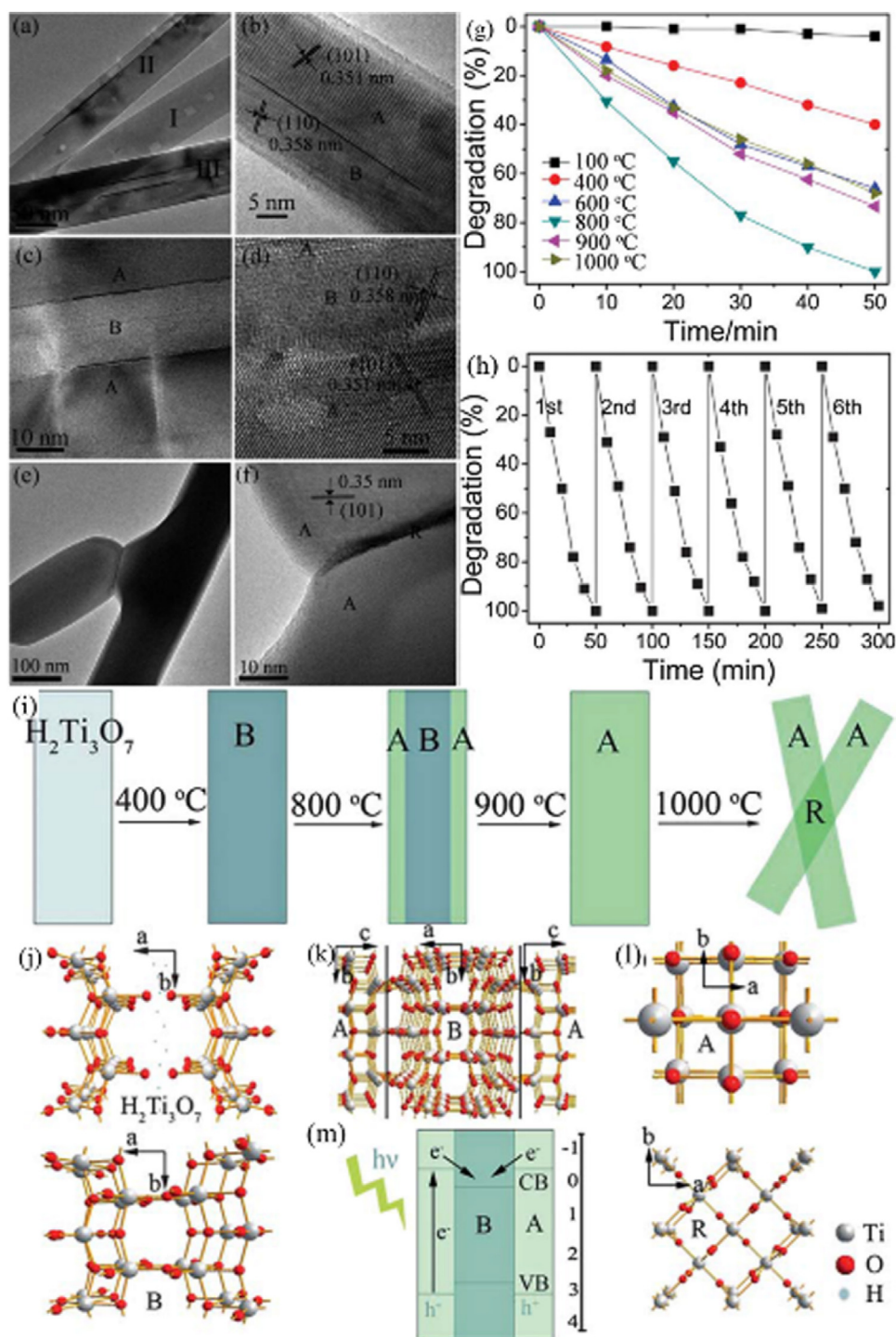
Fig. 10. Typical HRTEM images of (a)-(d) TiO$_2$(B)/anatase interface heterostructure NBs obtained at 800 °C and (e)–(f) rutile/anatase TiO$_2$ NBs obtained at 1000 °C; (g) Photocatalytic decomposition activity of TiO$_2$ NBs obtained by the different temperatures under UV light irradiation and (h) the photocatalytic stability of TiO$_2$(B)/anatase interface heterostructure NBs obtained at 800 °C; (i)–(m) A schematic view of the phase transformation mechanism of TiO$_2$ NBs, and the energy band matching and photogenerated charge carriers for the TiO$_2$(B)/anatase interface heterostructure TiO$_2$ NBs [62] Copyright 2011, The Royal Society of Chemistry.

(CSDD) process. First, the H$_2$Ti$_3$O$_7$ and C-H$_2$Ti$_3$O$_7$ NBs were dispersed into the Ni(NO$_3$)$_2$ solution for 5 h. Then, the soaked samples were collected and dried in an oven at 110 °C overnight, forming a layer of nickel nitrate on the NB surface. Finally, the dried samples were heated in a furnace at 600 °C for 2 h, with a heating speed of 1 °C min^{-1} to decompose the Ni(NO$_3$)$_2$ into NiO and transform the H$_2$Ti$_3$O$_7$ into TiO$_2$, thus forming NiO NP/TiO$_2$ NSHs and NiO NP/C-TiO$_2$ NSHs, as shown in Fig. 12a–d.

The uniform assembly of p-type NiO nanoparticles produces a large number of nano *p-n* junction heterostructures on the surface of the TiO$_2$ NBs, where NiO and TiO$_2$ act as the p- and n-type *n*-type semiconductors, respectively. Compared with both pure NiO nanoparticles and TiO$_2$ NBs, NiO-NP/TiO$_2$ NSHs and NiO-NP/C-TiO$_2$ NSHs exhibit a significantly enhanced photocatalytic activity, and the optimal NiO-NP/C-TiO$_2$ NSHs possess the highest photocatalytic activity under both UV and visible light irradiation, as shown
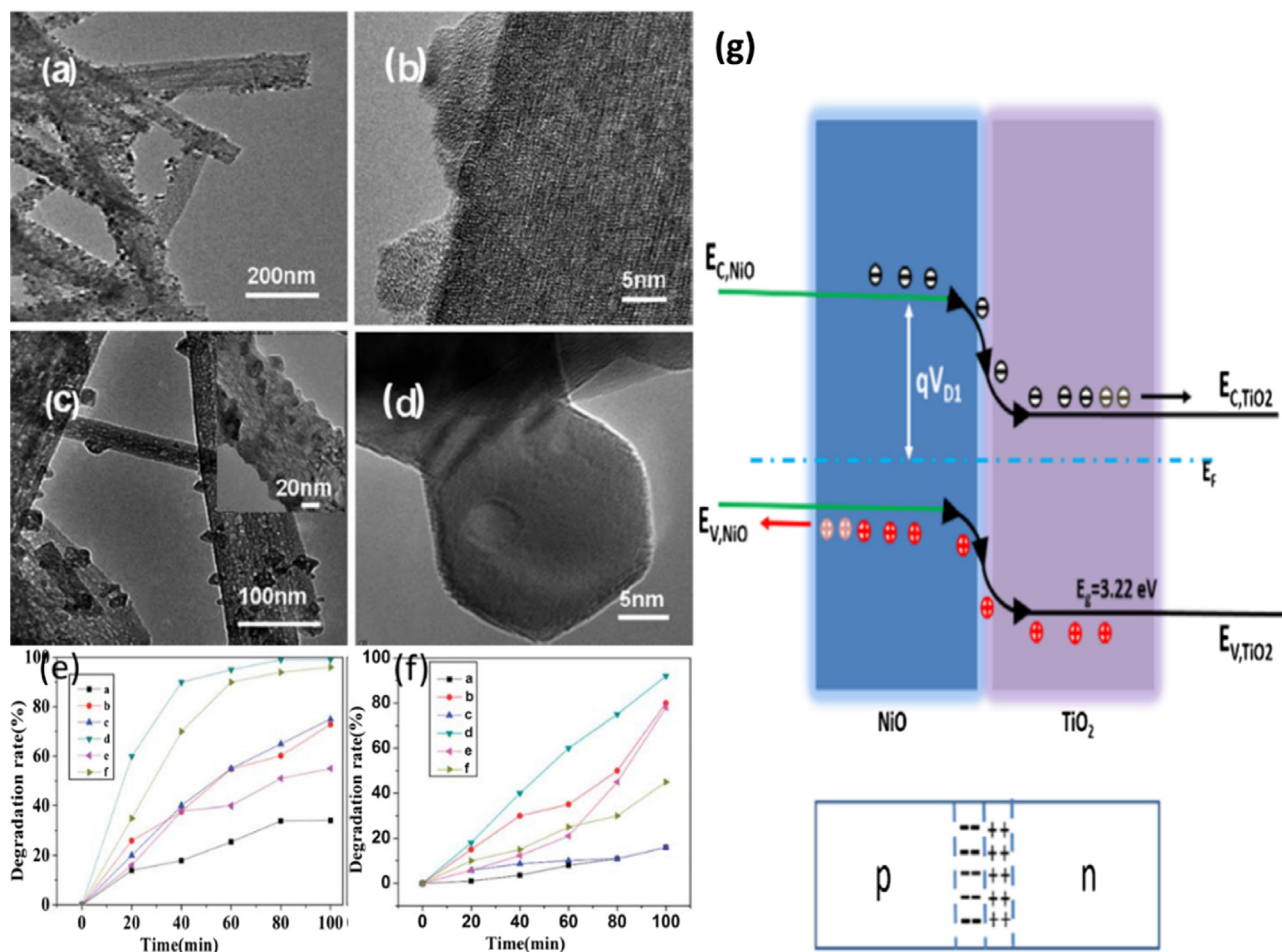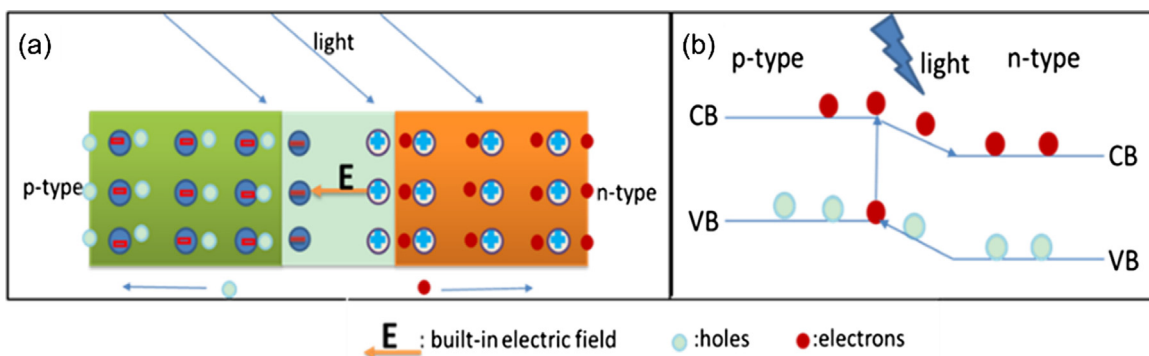
Fig. 11. Schematic diagram of the electron-hole separation process in the *p-n* junction (type-II) under irradiation: (a) space distribution of charge carriers; (b) band structure of *p-n* junction (CB: conduction band; VB: valence band).

Fig. 12. Representative TEM and HRTEM images of (a)-(b) NiO-NP/TiO$_2$ NSHs and (c)-(d) NiO-NP/C-TiO$_2$ NSHs. The (e) UV light and (f) visible light photocatalytic degradation rate of MO with different photocatalysts: a. pristine TiO$_2$ NBs, b. NiO-NP/TiO$_2$ NSHs, c. C-TiO$_2$ NBs, d. NiO-NP/C-TiO$_2$ NSHs, e. pure NiO nanoparticles, f. P25 [83] Copyright 2011, The Royal Society of Chemistry. (g) Schematic diagrams for the formation of a *p-n* nanojunction [84] Copyright 2015, Elsevier Ltd.

in Fig. 12e–f. It appears that the *p-n* junctions effectively reduce the recombination of charge carriers, which enhances the photocatalytic properties of the TiO$_2$ NBs, as shown in Fig. 12g. The C-TiO$_2$ NBs provide a larger number of photocatalytically active surfaces, which increases the photo-absorption, builds up the production of electron-hole pairs, and enhances the photocatalytic performance [95].

However, the *p-n* junction effect is limited because the built-in electric field can be saturated as a result of charge accumulation during the photocatalysis process. On the basis of Lin's work, Yu et al. synthesized double-shelled NiO/rGO/TiO$_2$ heterostructured coaxial nanocables by coating rGO nanosheets on electrospun NiO nano-fibers, and then assembling a layer of TiO$_2$ nanowires on top [84]. In this way, the photo-induced charge carriers can be
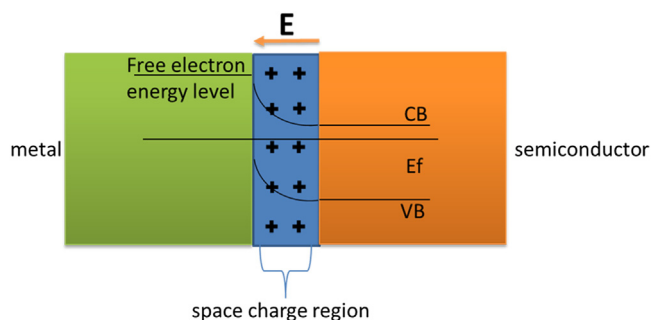
Fig. 13. Schematic of a Schottky junction.

separated faster, and the photocatalytic performance can be significantly enhanced.

4.3. TiO₂ NSHs based on the Schottky junction

4.3.1. The formation and properties of Schottky junctions

The Schottky junction is a type of simple heterostructure between a metal and semiconductor (for example the n-type semiconductor). Similar to *p-n* junctions, Schottky junctions also possess nonlinear impedance characteristics, which can promote charge carrier separation. Due to these properties, they can be used for photocatalysts, gas sensors [96], electron devices and so on.

The work functions of semiconductors are generally lower than those of metals. When a material with a Schottky junction is irradiated, photo-induced electrons can easily move from the semiconductor into metal, and the holes remain in the semiconductor. Therefore, the photo-induced charge carriers can be separated and the photocatalytic activity can be significantly promoted. Similar to the built-in electron field in *p-n* junctions, there is an electron field in Schottky junctions whose direction is from the semiconductor to metal. This electron field can prevent subsequent electrons from moving into metal, and the band near the interface is bent; the interface band acts as a high barrier and is called a Schottky barrier (Fig. 13). Only electrons that possess an energy higher than the Schottky barrier can move to the metal. When there is a balance, the height of Schottky barrier is equal to the D-value of the work function of the metal and semiconductor. In summary, a Schottky junction is similar to a *p-n* junction in promoting carrier separation and enhancing the photocatalytic efficiency [97].

To date, many types of metal/TiO₂ NSHs, such as Pt/TiO₂ NSHs [98], Pd/TiO₂ NSHs [99], Au/TiO₂ NSHs [100,101] and Ag/TiO₂-P/TiO₂-B double NSHs [71]. These metal/TiO₂ NSHs exhibit enhanced photocatalytic activity, in which the Schottky junction plays a determinative role in promoting the separation of photo-induced carriers.

Metal nanoparticle/TiO₂ NB heterostructures with different metal nanoparticles can be synthesized through different approaches, but their synthesis mechanisms are very similar. Therefore, we use Ag/TiO₂ NB heterostructures as an example to illustrate the TiO₂ NB-based Schottky-junction photocatalysts.

4.3.2. Ag/TiO₂ NSHs

Based on the TiO₂-P/TiO₂-B synthesized by the acid-etching process mentioned above, Zhou et al. prepared Ag/TiO₂-P/TiO₂-B double NSHs by a photo-reduction process that can dramatically enhance the photocatalysis properties of TiO₂ NBs [71]. The synthesis process is based on the photoreduction property of TiO₂ NBs; it is facile, low-cost and timesaving. The typical synthesis procedure is as follows: 10 mL of 0.1 M AgNO₃ ethanol solution is mixed with 0.02 g of TiO₂-P/TiO₂-B NBs to form a suspension. The system is irra-

diated by UV light under magnetic agitation for 1 min. The collected powders are the Ag/TiO₂-P/TiO₂-B NB surface heterostructures.

As shown in Fig. 14a and b, most of the Ag nanoparticles are loaded on the outmost surface of the TiO₂-nanoparticles of the TiO₂-P/TiO₂-B NBs, where the surface energy is higher than the energy at the flat position of the TiO₂ NBs; they form a double-heterostructured Ag/TiO₂-P/TiO₂-B NSHs. The bottom heterostructure is TiO₂-P/TiO₂-B with the same composition, and the top heterostructure is Ag nanoparticle/TiO₂ nanoparticle heterostructure with a Schottky junction. From the MO solution degradation results (Fig. 14e), it is clear that the TiO₂ NBs possess the lowest photocatalytic activity, and can only degrade 76% of the MO under UV light irradiation in 60 min, while the TiO₂-P/TiO₂-B single-heterostructures can degrade 100% of MO in 50 min. The Ag/TiO₂-P/TiO₂-B double-heterostructures possess the highest photocatalytic activity, which can degrade 100% of MO in 30 min.

The enhanced photocatalytic performance of Ag/TiO₂-P/TiO₂-B in comparison to TiO₂-P/TiO₂-B can be mainly attributed to the Schottky junctions, in which the Ag nanoparticles can serve as an efficient electron trap that favors the interfacial charge transfer between the metal and semiconductor and the separation of photo-generated e⁻/h⁺ pairs. As a result, the electron density in the Ag particles and the hole density in TiO₂ are increased, leading to a significantly improved photocatalytic activity. In summary, the enhancement of the photocatalytic activity is attributed to the heterostructures that combine the TiO₂ nanoparticles, TiO₂ NBs and Ag nanoparticles, which are controlled by energy band matching and the Schottky barrier effect. In addition, the rough surface of the structure provides abundant active sites, which can also improve the photocatalytic performance.

4.4. TiO₂ NSHs to broaden the photocatalytically active light region

In addition to forming *p-n* junctions and Schottky junctions to promote the separation of charge carriers, another important reason for loading the second phase on the surface of TiO₂ NBs is to broaden the light absorption region. As mentioned above, TiO₂ only possesses UV-light photocatalysis due to its intrinsic wide band gap. Therefore, TiO₂ NBs modified by metal oxides with visible- or even IR-light sensitization capability to form heterostructures is an effective method to improve photocatalytic activity [102]. Based on the principles above, many types of semiconductor/TiO₂ NSHs, such as Ag₂O/TiO₂ [102–104], PdO/TiO₂ [88], MoS₂/TiO₂ [26,57], CeO₂/TiO₂ [76], RuO₂/TiO₂ [105], and Sn₃O₄/TiO₂ [106] NSHs [107,108] have been designed and synthesized.

4.4.1. Ag₂O/TiO₂ NSHs

Zhou et al. synthesized two types of Ag₂O/TiO₂ NSHs by a simple physical mixing method (Fig. 15) [103] and a chemical co-precipitation method (Fig. 16) [89], respectively.

In the physical mixing method, the common TiO₂ NBs and Ag₂O nanoparticles are prepared independently. The pure Ag₂O nanoparticles were synthesized by a precipitation method using AgNO₃ and NaOH aqueous solution. A Ag₂O/TiO₂ heterostructure with a weight ratio of 1:1 was prepared by a simple physical mixing at room temperature. 0.1 g TiO₂ NBs and 0.1 g Ag₂O nanoparticles were physically well mixed and then stirred uniformly. The mixture obtained was not heat-treated or grinded further.

The photocatalysis activity of this type of Ag₂O/TiO₂ NSH was tested under UV light irradiation. In the photocatalysis reaction, Ag₂O nanoparticles can absorb the valence electrons of the TiO₂ NBs to enhance electron-hole separation and thus create a high interface-dominated photocatalytic activity.

Therefore, another type of Ag₂O/TiO₂ heterostructure with a high photocatalytic activity in both the UV and visible-light regions
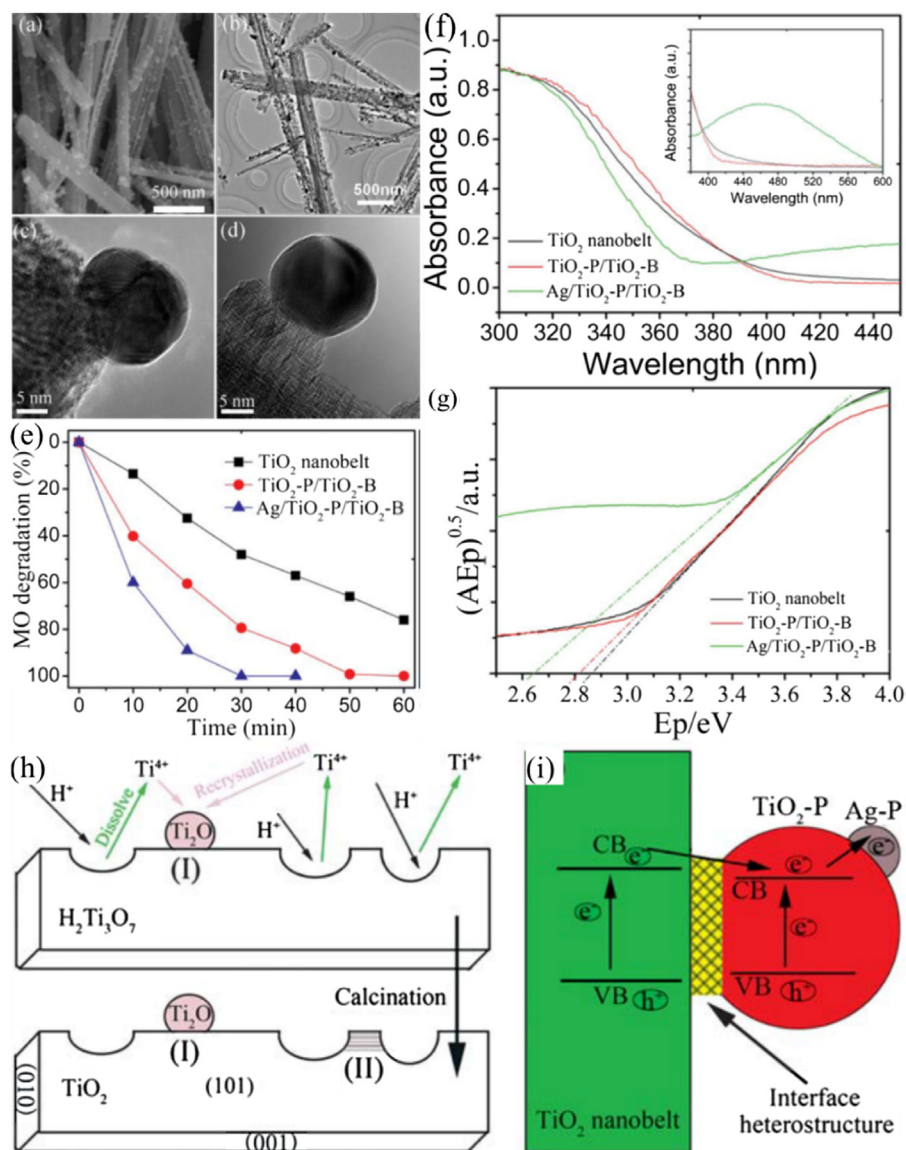
Fig. 14. (a) SEM and (b)–(d) HRTEM images of the Ag/TiO$_2$-P/TiO$_2$-B double- heterostructure; (e) Photocatalytic decomposition results of TiO$_2$ NBs (600 °C), TiO$_2$-P/TiO$_2$-B heterostructures (12 h, 600 °C) and Ag/TiO$_2$-P/TiO$_2$-B heterostructures under UV light irradiation; (f) UV–vis DRS and (g) the plots of $(\alpha E_p)^{0.5}$ *versus* E_p of TiO$_2$ NBs (600 °C), TiO$_2$-P/TiO$_2$-B heterostructures (12 h, 600 °C) and Ag/TiO$_2$-P/TiO$_2$-B heterostructures; (h)–(i) A schematic view of the formation mechanism, energy band matching and electron-hole separation of Ag/TiO$_2$-P/TiO$_2$-B heterostructures under UV light irradiation [71] Copyright 2011, The Royal Society of Chemistry.

was synthesized via a chemical co-precipitation method by using C-TiO$_2$ NBs as the substrate materials [102]. A typical process of creating Ag$_2$O/TiO$_2$ NBs with a weight ratio of 1:1 is as follows: 0.2 g of C-TiO$_2$ NBs was dispersed in 50 mL of distilled water, and 0.29 g of AgNO$_3$ was added to the suspension. The mixture was stirred magnetically for 30 min. Then, 50 mL of 0.2 M NaOH was dropped into the mixture of AgNO$_3$ and TiO$_2$. The NaOH was in excess, and the final pH was 14. Finally, the Ag$_2$O nanoparticle-decorated TiO$_2$ NBs were washed thoroughly with deionized water, and a filtration and drying process followed.

The Ag$_2$O/TiO$_2$ NSH is a photocatalyst with high activity for the degradation of MO under both UV and visible light irradiation. However, the mechanisms of the photocatalytic activity under UV and visible light are different. Under UV-light irradiation, Ag$_2$O nanoparticles absorb the electrons of TiO$_2$ NBs to enhance the electron-hole separation. The valence holes of TiO$_2$ NBs are consumed on the surface of TiO$_2$ to produce •OH radicals. Under visible light irradiation, Ag$_2$O nanoparticles on TiO$_2$ NBs as the visible-light active component enhanced the photocatalytic activity of the

Ag$_2$O/TiO$_2$ heterostructure via synergetic effects on the thermocatalytic activity and efficient electron transmission at the Ag$_2$O/TiO$_2$ interface.

4.4.2. Scaly Sn$_3$O$_4$/TiO$_2$ NSHs

Another sample used for UV–vis light wide-band gap NSHs are the scaly Sn$_3$O$_4$/TiO$_2$ NSHs reported by Chen et al. [106], which shows enhanced photocatalysis efficiency under both UV and visible light irradiation. The scaly Sn$_3$O$_4$ nanoflakes were chemically synthesized in situ and assembled on C-TiO$_2$ NBs.

The C-TiO$_2$ NBs were used as the substrate to load Sn$_3$O$_4$. The scaly Sn$_3$O$_4$/TiO$_2$ NSHs were prepared by a hydrothermal co-precipitation method. In a typical process, 5.0 mmol SnCl$_2$·2H$_2$O and 12.5 mmol Na$_3$C$_6$H$_5$O$_7$·2H$_2$O were dissolved in 12.5 mL of deionized water and a certain amount of C-TiO$_2$ NBs (molar ratio of Sn/Ti = 1/1, 2/1 and 3/1) was added to the solution. Then, 12.5 mL of 0.2 M NaOH aqueous solution was used as the precipitating agent. The solution was transferred into a 50 mL Teflon-lined stainless steel autoclave and maintained at 180 °C for 12 h. The Sn$_3$O$_4$/TiO$_2$
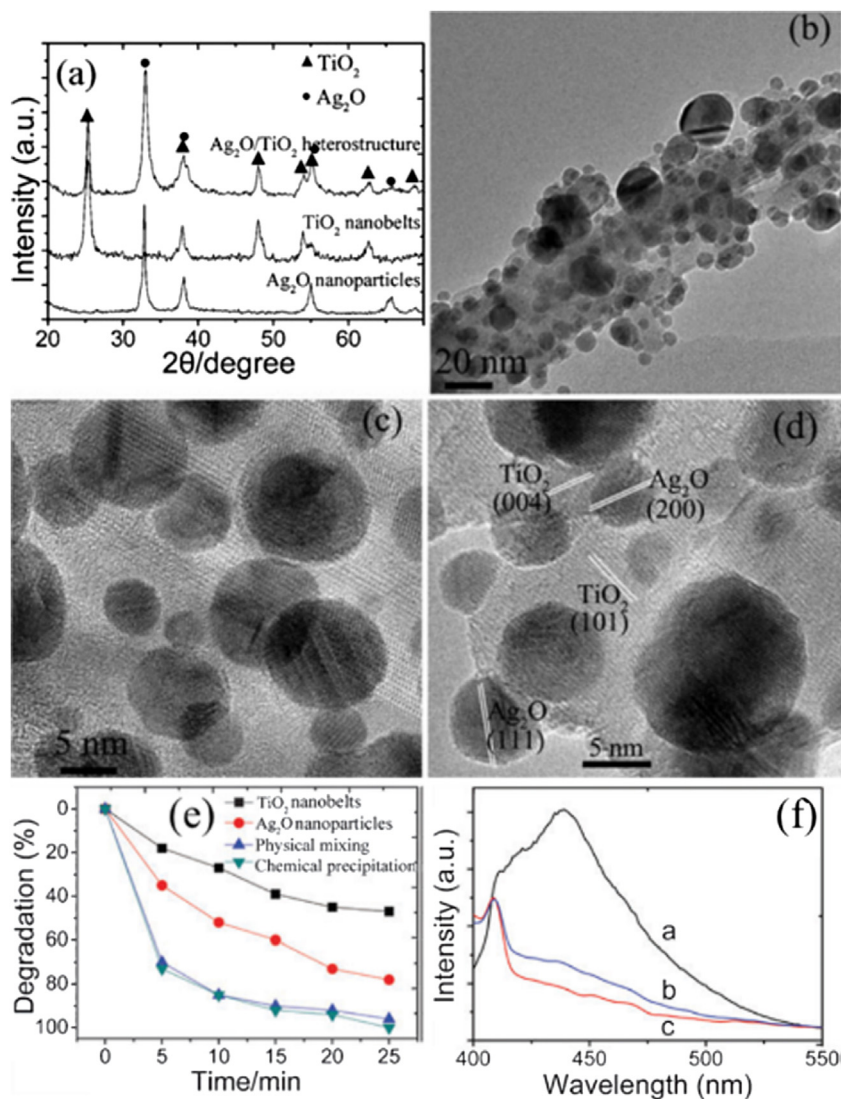
Fig. 15. (a) XRD patterns and (b)–(d) HRTEM images of the as-synthesized Ag_2O/TiO_2 NB heterostructure; (e) UV light photocatalytic degradation of MO solution in the presence of Ag_2O nanoparticles, TiO_2 NBs and Ag_2O/TiO_2 heterostructure obtained by physical mixing and chemical precipitation [103] Copyright 2010, the Owner Societies.
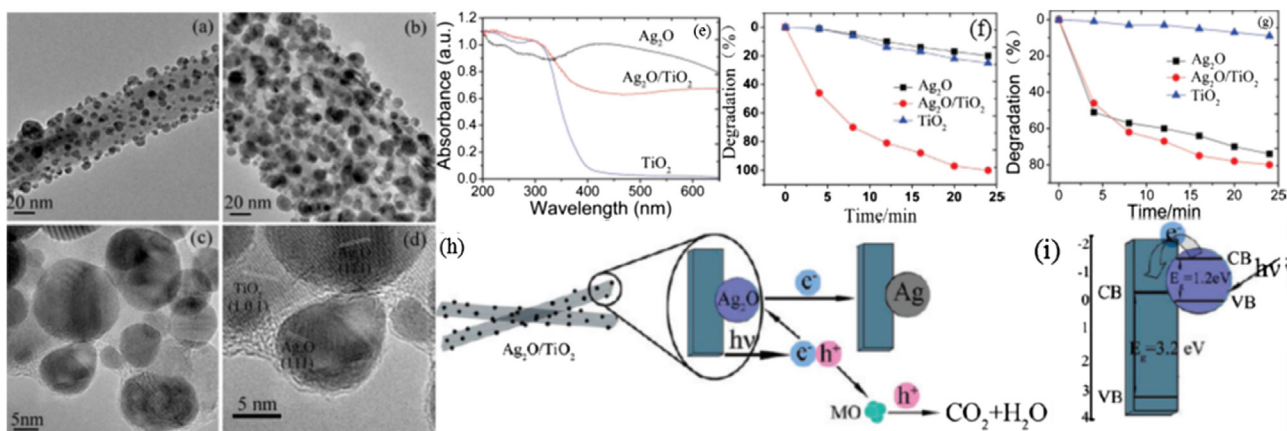

Fig. 16. (a)-(d) HRTEM images of Ag_2O/TiO_2 NBs (1:1) with different magnifications; (e) UV–vis DRS of TiO_2 NBs, Ag_2O/TiO_2 heterostructure, and Ag_2O nanoparticles; Photocatalytic degradation of MO in the presence of Ag_2O, Ag_2O/TiO_2 heterostructures, and TiO_2 NBs under (f) UV light and (g) visible light irradiation [102] Copyright 2010, American Chemical Society.
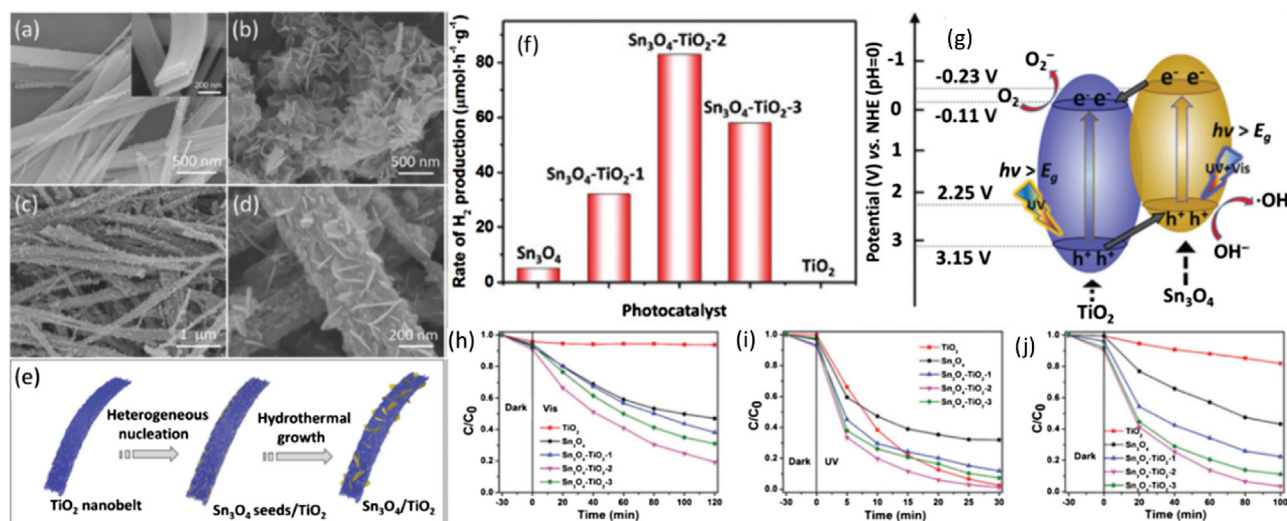
Fig. 17. SEM images of (a) C-TiO$_2$ NBs; the inset in (a) is the TiO$_2$ NB before acid treatment; (b) Sn$_3$O$_4$ nanoflakes; (c)–(d) Scaly Sn$_3$O$_4$/TiO$_2$ NB heterostructures; (e) Schematic illustration of the synthetic process of the Sn$_3$O$_4$/TiO$_2$ heterostructure; (f) Comparison of the photocatalytic hydrogen evolution activities of different samples; (g) Schematic diagram of electron transfer in the Sn$_3$O$_4$/TiO$_2$ heterostructure; Photocatalytic degradation of MO aqueous solution by TiO$_2$ NBs, Sn$_3$O$_4$ nanoflakes and Sn$_3$O$_4$/TiO$_2$ heterostructures (molar ratio of Sn/Ti = 1/1, 2/1, and 3/1) under (h) visible light, (i) UV light and (j) simulated solar spectrum irradiation [106] Copyright 2015, The Royal Society of Chemistry.

NSHs were obtained after washing with deionized water and ethanol, and the NSHs were dried at 60 °C for 12 h.

The Sn/Ti molar ratio of the reactants can influence the morphology and distribution of Sn$_3$O$_4$ nanoflakes, and Sn$_3$O$_4$/TiO$_2$ heterostructures with a molar ratio of Sn/Ti of 2/1 exhibited the highest photocatalytic activity. Compared with single-phase nanostructures of Sn$_3$O$_4$ and TiO$_2$, the Sn$_3$O$_4$/TiO$_2$ NSHs exhibited a markedly enhanced photocatalytic hydrogen evolution even without the Pt co-catalyst, and they enhanced the degradation ability of MO under both UV and visible light irradiation. The outstanding performance is ascribed to three aspects: the increased exposure of active facets, the broad light absorption and the matching energy band structure between Sn$_3$O$_4$ and TiO$_2$, which improved the separation and the lifetime of photo-induced charge carriers. The assembly of Sn$_3$O$_4$ broadened the photoactive range of the TiO$_2$ NBs into the visible light region (Fig. 17).

Some other very important works on TiO$_2$ NSHs, such as MoS$_2$ nanosheet/TiO$_2$ NB heterostructures [26,57] and reduced graphene oxide nanosheet/TiO$_2$ NB heterostructures [109] with enhanced photocatalytic properties, will not reviewed in this paper.

4.5. UV–vis-NIR-light photocatalysis based on TiO$_2$-based NB surface heterostructures

Although the fabrication of the TiO$_2$-based heterostructures mentioned earlier have broadened the photocatalytic activity of TiO$_2$ from the UV light to the visible spectrum regions, there is ongoing research on materials and methods for full solar-light photocatalysis because the near-infrared (NIR) light, which makes up approximately more than 50% of the solar spectrum, remains unutilized. As is well known, it is difficult for semiconductors to use NIR light (with its low photoenergy) directly due to their band-gap width and the VB and CB positions. To utilize solar energy more efficiently, numerous efforts have been made to develop photocatalysts that can harvest the wide spectrum of solar light, from the UV to NIR wavelengths. Doping rare earth ions into the traditional photocatalysts is an effective method of achieving this. Doping of Yb^{3+} and Tm^{3+} into TiO$_2$ [110,111] has been conducted to achieve photocatalytic activity of NIR-light due to the up-conversion effect; the photocatalytic activity was evaluated under irradiation by 980 nm

NIR light. The dopants can serve as an intermedium, transferring energy to the UV- or visible-light-active photocatalysts to generate strongly oxidative holes and reductive electrons that are essential for continuing the photocatalytic reaction. [112,113] Unfortunately, the efficient utilization of sunlight is limited due to the photocatalyst's very narrow absorption band of light at 980 nm [10,13]. Hydrogenation is another facile and effective way to obtain narrow-bandgap photocatalysts, with black hydrogenated TiO$_2$ (H-TiO$_2$) as a typical example [2,114]. However, it is still extremely difficult for a single photocatalyst to efficiently utilize the full spectra of solar light. Until now, only a few NIR photocatalysts have been studied, such as Bi$_2$WO$_6$ [23,115], Cu$_2$(OH)PO$_4$ [116], WS$_2$ [109] and In$_2$S$_3$ [117], which are usually used as broadband spectrum photocatalysts to promote significant activity. However, most of IR photocatalysts above possess poor UV photocatalytic activity. As mentioned above, assembling IR photocatalytic nanoparticles on the surface of TiO$_2$ NBs is a practical way to synthesize full solar light spectrum photocatalysts.

In the following section, we will introduce two types of TiO$_2$ NSHs as examples to illustrate the full solar light spectrum photocatalysts.

4.5.1. Bi$_2$WO$_6$/TiO$_2$ NB heterostructures

Recently, we found that Bi$_2$WO$_6$ nanosheets possess good IR photocatalytic activity, which is derived from their impurity energy level due to the oxygen vacancies in Bi$_2$WO$_6$ [23].

By assembling Bi$_2$WO$_6$ on TiO$_2$ NBs through the hydrothermal process, Bi$_2$WO$_6$/TiO$_2$ NB heterostructures Bi$_2$WO$_6$/TiO$_2$ NSHs with UV-vis-NIR full solar spectrum photocatalytic activity were prepared. Typically, 0.2-0.8 mmol of Bi(NO$_3$)$_3$·5H$_2$O and 0.1-0.4 mmol of Na$_2$WO$_4$·2H$_2$O were blended uniformly in 40 mL of ethylene glycol or nitric acid and 1.2 mmol of TiO$_2$ NBs was dispersed into the solution above. The as-prepared solution was then transferred into a Teflon-lined autoclave and heated at 160 °C for 15 h.

To obtain high UV light photocatalytic performance, the TiO$_2$ NBs used for building Bi$_2$WO$_6$/TiO$_2$ NB heterostructures were coarsened by acid treatment to enlarge the UV active surface of the NBs [23]. As shown in Fig. 18, Bi$_2$WO$_6$ nanoparticles are assembled on surface of TiO$_2$ NBs with a teeth-like nanosheet morphology growing out from the surface of TiO$_2$. This novel nanostructure not
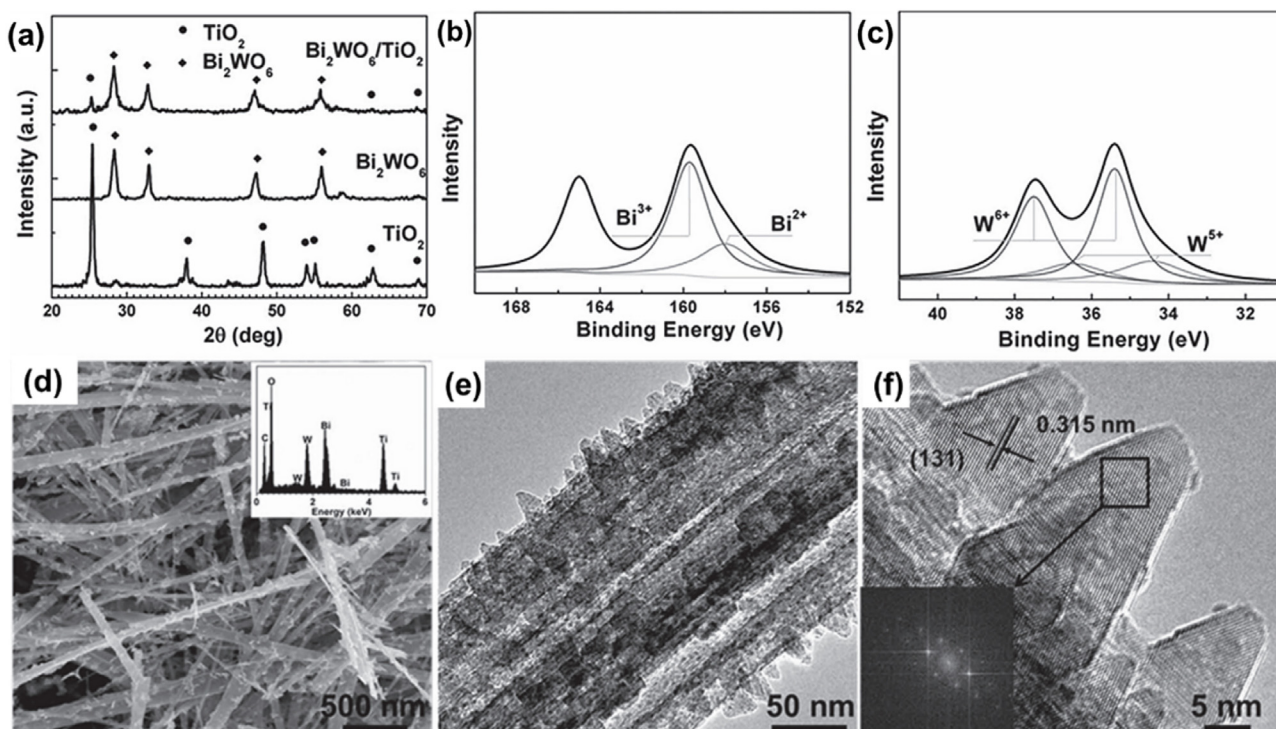
Fig. 18. (a) XRD patterns of TiO_2 NBs, Bi_2WO_6 nanosheets and Bi_2WO_6/TiO_2 NSHs. (b) Bi_{4f} and (c) W_{4f} core-level XPS spectra of Bi_2WO_6/TiO_2 NSHs; (d) SEM image and (e)–(f) TEM images of Bi_2WO_6/TiO_2 NSHs (14 wt% Bi_2WO_6). The energy-dispersive X-ray spectroscopy (EDS) of Bi_2WO_6/TiO_2 NSHs is shown in the top inset of (d) [23] Copyright 2013, WILEY-VCH Verlag GmbH & Co. KGaA, Weinheim.

only can absorb NIR and visible light based on the visible-NIR photocatalytic activity but also retains a high UV activity because the teeth-like nanosheets on TiO_2 NBs do not block UV light irradiation.

A photocatalysis assessment of Bi_2WO_6, TiO_2 NB, and Bi_2WO_6/TiO_2 NSHs proved that among all the three samples, Bi_2WO_6/TiO_2 NSHs not only has the best UV light activity but also it has the best visible and NIR photocatalytic activity. This behavior is not only attributed to the synergy effect of the visible-NIR photocatalytic activity of Bi_2WO_6 and the UV photocatalytic performance of TiO_2 but also attributed to the enhancement of the photo-induced carrier separation (Fig. 19).

4.5.2. CQDs/H-TiO$_2$ NB heterostructures

Another example of a full solar spectrum photocatalyst is the work on carbon quantum dot/hydrogenated TiO_2 (CQDs/H-TiO_2) NB heterostructures [118]. As the substrate of the CQDs/H-TiO_2 hybrid photocatalyst, H-TiO_2 possesses a high UV and visible light photocatalytic property. It is believed that surface disorder and oxygen vacancies can be introduced into the surface of anatase TiO_2 NBs by hydrogenation (H-TiO_2), leading to the formation of Ti^{3+} centers or unpaired electrons, followed by the formation of donor levels in the electronic structure of TiO_2 [119,120]. Oxygen vacancies are believed to be the key factor for suppressing the recombination of photoinduced electrons and holes, which can efficiently improve the photocatalytic activity of TiO_2 [121,122]. At the same time, the impurity band caused by the oxygen vacancies endows the hydrogenated TiO_2 NBs with visible light photocatalytic activity. On the other hand, carbon quantum dots possess excellent up-conversion photoluminescence (PL), which can convert a broad region of near-infrared light into visible light (Fig. 20). As was intended, the visible light converted by the CQDs can be absorbed by H-TiO_2 and used for photocatalysis. In addition, the CQDs can work as electron acceptors and enhance the photo-induced carrier separation because of their high work function [123,124]. Based on the design mechanism above, CQDs/H-TiO_2

heterostructures were prepared, and their photocatalytic properties were assessed.

The TiO_2 NBs were obtained by the hydrothermal process mentioned previously, while the H-TiO_2 NBs were produced by annealing the corroded TiO_2 NBs in hydrogen atmosphere at 600 °C for 60 min; this was performed in a tube furnace filled with a mixture of hydrogen and argon gas (1:1). While the CQDs were synthesized by a facile one-step alkali-assisted ultrasonic treatment using glucose as the precursor. To form the heterostructures, H-TiO_2 NBs were added to an aqueous solution of CQDs and treated with an oil bath reflux at 90 °C for 3 h. The heterostructures were then washed thoroughly with water and dried in an oven at 60 °C for 12 h.

The TEM (Fig. 20a) image shows the spherical CQDs particles with a diameter of less than 5 nm and good monodispersity. As is shown in Fig. 20c-d, both the low-magnification and high-magnification TEM images show the obvious hybrid structure, in which the TiO_2 NB is homogeneously covered with a dense CQDs layer.

The assessment of the photocatalytic performance of the samples proved that TiO_2 NBs just possess UV light photocatalytic activity, H-TiO_2 NBs have acceptable UV–vis light photocatalysis performance, and the CQDs/H-TiO_2 hybrid photocatalyst is endowed with full solar spectrum photocatalytic activity, including in the UV, visible and near-infrared light region (Fig. 21) [118].

The above examples for TiO_2 NSHs with the UV-vis-NIR light photocatalytic property open a door for building photocatalysts with full use of the solar energy spectrum. This basic idea will attract more and more attention of materials scientists and environmental engineers.

5. Conclusion and prospects

Assembling second-phase nanoparticles on TiO_2 NBs to form TiO_2 NB surface heterostructures has been widely applied for the
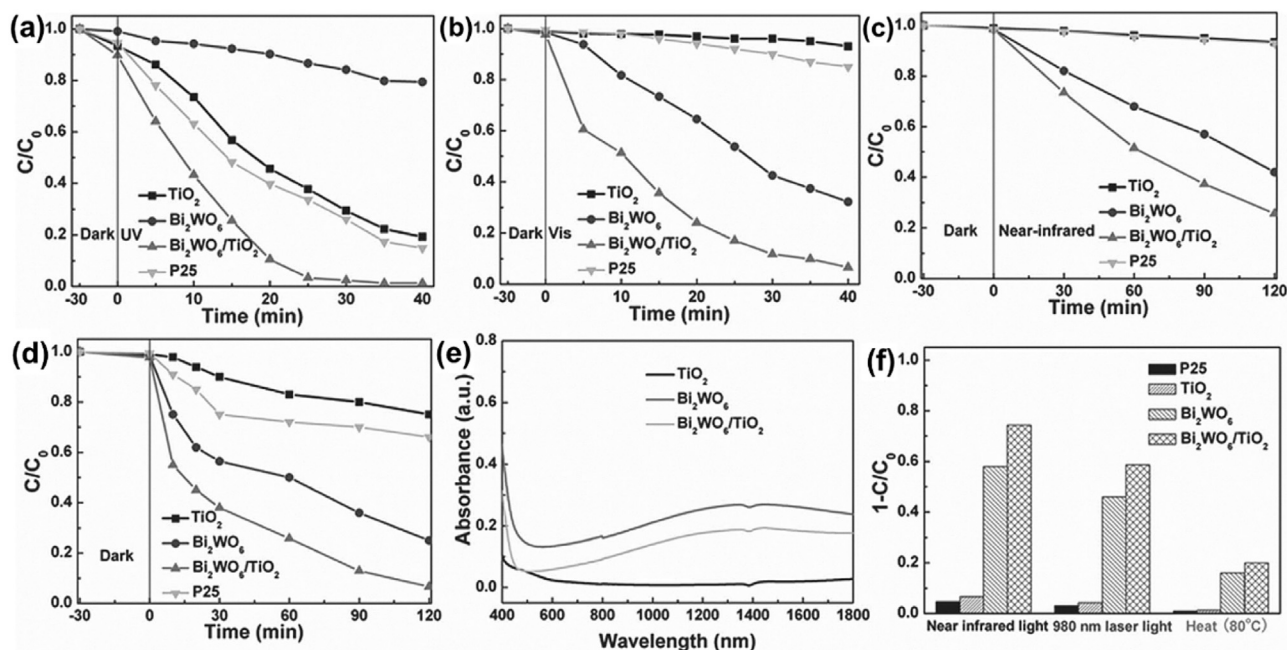
Fig. 19. Photocatalytic degradation of MO under (a) UV light, (b) visible light, (c) NIR light and (d) simulated sunlight irradiation; (e) Visible and NIR absorption spectrum of TiO$_2$ NBs, Bi$_2$WO$_6$ nanosheets and Bi$_2$WO$_6$/TiO$_2$ heterostructures; (f) Photocatalytic degradation of MO under NIR light irradiation, 980 nm laser light irradiation, and heat at 80 °C in the dark for 120 min [23] Copyright 2013, WILEY-VCH Verlag GmbH & Co. KGaA, Weinheim.
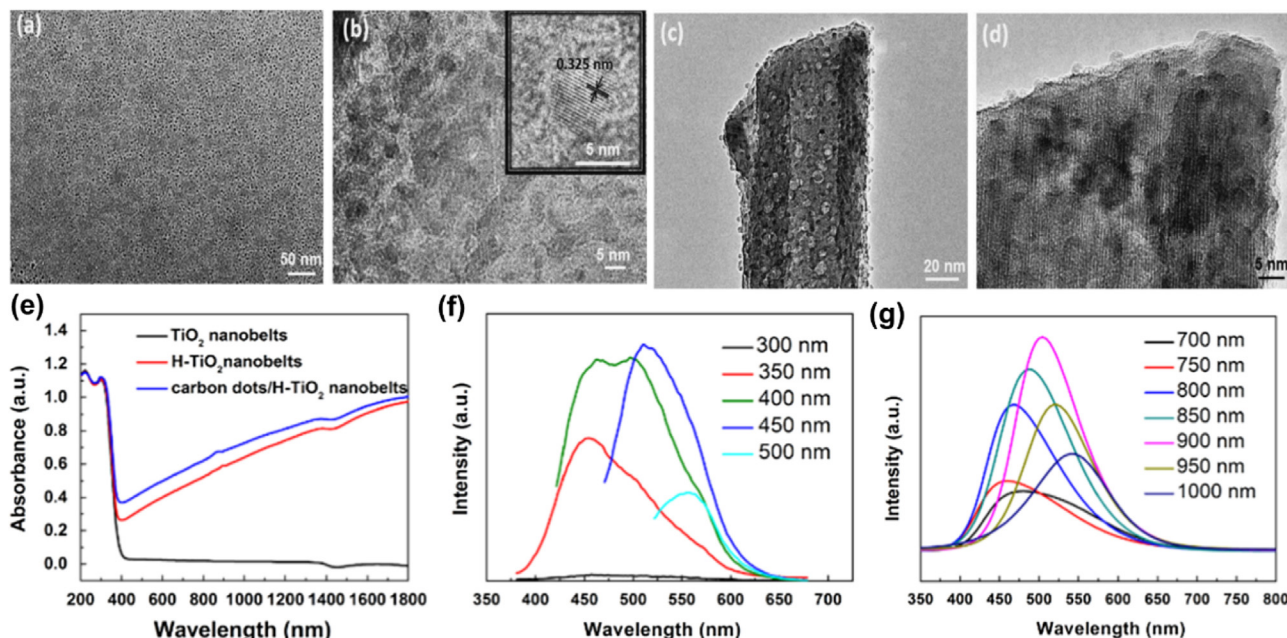

Fig. 20. (a) Low-magnification and (b) high-magnification TEM images of CQDs (Insets: HRTEM images); (c) low-magnification and (d) high-magnification TEM images of CQDs/H-TiO$_2$ heterostructures; (e) UV–vis–NIR diffuse reflectance spectra of TiO$_2$ NBs, H-TiO$_2$ NBs, and CQDs/H-TiO$_2$ heterostructures; (f) down-converted and (g) up-converted photoluminescence spectra of CQDs [118]. Copyright 2014, Elsevier Ltd.

construction of high-performance photocatalysts because the well-designed TiO$_2$ nanobelt surface heterostructures can overcome many of the problems of single-phase semiconductor photocatalysts. Therefore, TiO$_2$ NSHs have become a powerful tool for building new hybrid photocatalysts, which can be used in different photocatalytic reactions, such as photodegradation of organic pollutants, photocatalytic water-splitting for hydrogen generation, photocatalytic reduction of CO$_2$, and green synthesis chemistry. As a broad bandgap semiconductor, TiO$_2$ NB can be integrated with many other types of semiconductors or metals to form TiO$_2$ NSHs,

which provide a great platform for the design of new photocatalysts with a belt-like morphology. At present, the research on TiO$_2$ NSHs has just begun, and this field will attract more attention in the next few years, which will result in great advances in the development of photocatalysts and photocatalysis for solar applications.

On the basis of the studies above, several important aspects should be taken into consideration in developing future research: 1) a clear understanding of the growth mechanism of TiO$_2$ NBs, to obtain products with biphasic compositions and more active sites while maintaining their typical morphology; 2) the design and
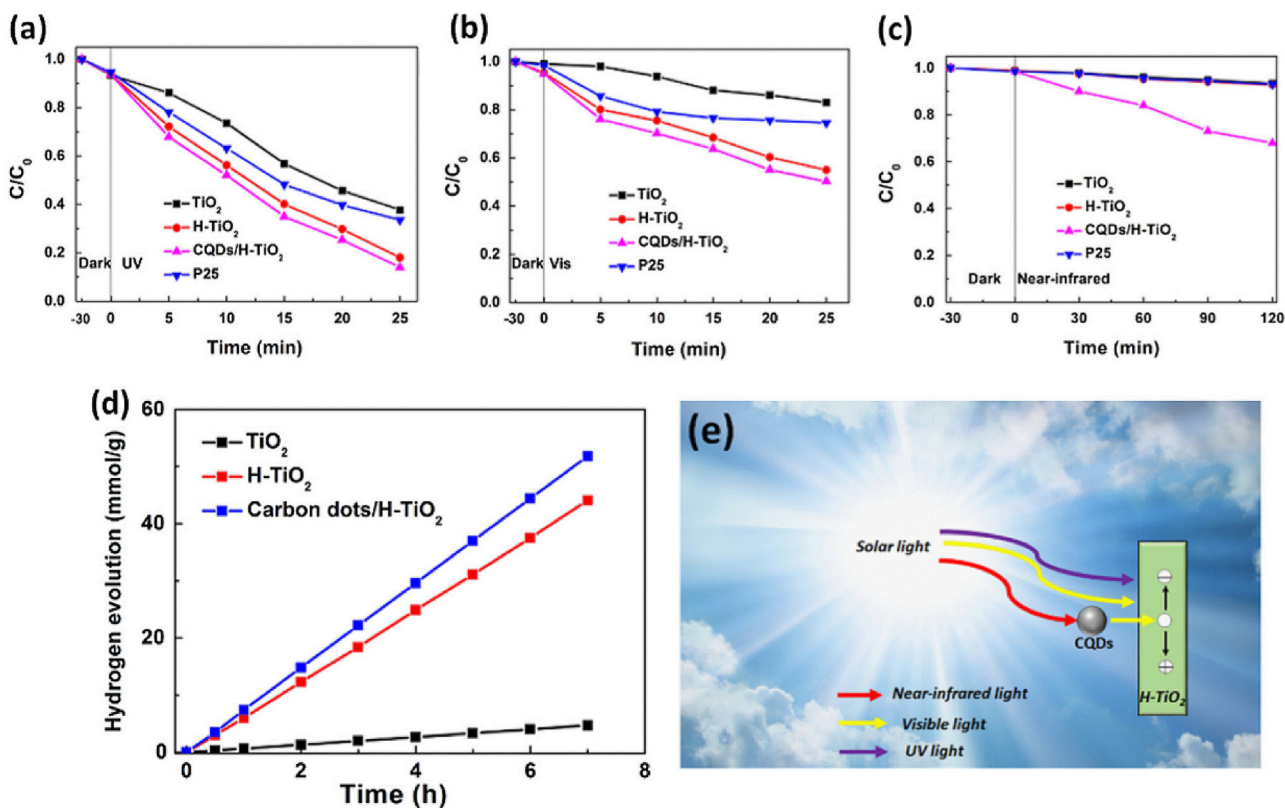
Fig. 21. Photocatalytic degradation of MO in the presence of P25, TiO$_2$ NBs, H-TiO$_2$ NBs and CQDs/H-TiO$_2$ heterostructures under (a) UV, (b) visible, and (c) NIR light irradiation; (d) Photocatalytic hydrogen generation of 1 wt% Pt-loaded TiO$_2$ NBs, H-TiO$_2$ NBs, and CQDs/H-TiO$_2$ heterostructures under a Xe arc lamp (300 W); and (e) Schematic of photocatalytic mechanism for the CQDs/H-TiO$_2$ heterostructures under UV, visible and NIR light irradiation [118] Copyright 2014, Elsevier Ltd.

fabrication of visible- and infrared-light photocatalysts with high performance to obtain high-performance photocatalysts that have a light response in the full solar light spectrum; 3) an increase in the light absorption efficiency for TiO$_2$-based NB surface heterostructures for practical applications.

Semiconductor nanomaterials for photocatalysis have been studied for many years. However, most studies paid more attention to the photocatalytic mechanism and the means of obtaining high performance without considering the cost of manufacturing. In addition, most studies used artificial light sources and batch-by-batch photodegradation experiments. However, the cost, the morphology, the active light region of the photocatalysts, the high operation cost of artificial light sources, and the non-continuous photodegradation mode are great obstacles for practical applications in the water-treatment industry, which is a very promising field for photocatalysis. TiO$_2$ NSHs provide a facile and powerful tool for the design and mass-production of highly active, broad light spectrum and high performance photocatalysts that have great potential in the water-treatment industry, are important for photocatalytic polymerization and will benefit other industries with solar light acting as the light source. More recently, we have successfully designed and set-up a continuous industrial photocatalytic water treatment equipment. In addition, the experiments on advanced treatments of dyehouse waste have proven that TiO$_2$ NSHs are the perfect choice for industrial wastewater treatment.
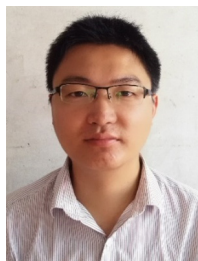
Acknowledgements

References

[1] G.G. Lenzi, R.F. Evangelista, E.R. Duarte, L. Colpini, A.C. Fornari, R. Menechini Neto, L. Jorge, O. Santos, Desalin. Water Treat. 57 (2016) 14132–14144.
[2] D. Yue, X. Qian, Y. Zhao, Sci. Bull. 60 (2015) 1791–1806.
[3] Y.H. Hu, Angew. Chem. Int. Ed. 51 (2012) 12410–12412.
[4] J. Liu, Y. Liu, N. Liu, Y. Han, X. Zhang, H. Huang, Y. Lifshitz, S. Lee, J. Zhong, Z. Kang, Science 347 (2015) 970–974.
[5] D. Kim, K.K. Sakimoto, D. Hong, P. Yang, Angew. Chem. Int. Ed. 54 (2015) 3259–3266.
[6] Y. Zhao, X. Jia, G.I. Waterhouse, L.Z. Wu, C.H. Tung, D. O'Hare, T. Zhang, Adv. Energy Mater. 6 (2016) 1501974.
[7] Y. Zhao, B. Zhao, J. Liu, G. Chen, R. Gao, S. Yao, M. Li, Q. Zhang, L. Gu, J. Xie, Angew. Chem. Int. Ed. 55 (2016) 4215–4219.
[8] S. Yamauchi, K. Yamamoto, S. Hatakeyama, J. Mater. Sci. Chem. Eng. 03 (2015) 28–38.
[9] H. Li, Y. Sun, B. Cai, S. Gan, D. Han, L. Niu, T. Wu, Appl. Catal. B: Environ. 170–171 (2015) 206–214.
[10] N. Lu, Y. Su, J. Li, H. Yu, X. Quan, Sci. Bull. 60 (2015) 1281–1286.
[11] J. Tian, Z. Zhao, A. Kumar, R.I. Boughton, H. Liu, Chem. Soc. Rev. 43 (2014) 6920–6937.
[12] S.G. Kumar, L.G. Devi, J. Phys. Chem. A 115 (2011) 13211–13241.
[13] Q. Li, B. Guo, J. Yu, J. Ran, B. Zhang, H. Yan, J.R. Gong, J. Am. Chem. Soc. 133 (2011) 10878–10884.
[14] L. Shang, B. Tong, H. Yu, G.I. Waterhouse, C. Zhou, Y. Zhao, M. Tahir, L.Z. Wu, C.H. Tung, T. Zhang, Adv. Energy Mater. 6 (2016) 1501241.
[15] Z. Meng, L. Zhu, S. Ye, Q. Sun, K. Ullah, K. Cho, W. Oh, Nanoscale Res. Lett. 8 (2013) 1–10.
[16] S. Khanchandani, S. Kundu, A. Patra, A.K. Ganguli, J. Phys. Chem. C 117 (2013) 5558–5567.
[17] B. Adeli, F. Taghipour, Appl. Catal. A: Gen. (2016).
[18] Z. Zhao, M. Miyauchi, Angew. Chem. Int. Ed. 47 (2008) 7051–7055.
[19] W. Zhou, H. Liu, J. Wang, D. Liu, G. Du, J. Cui, ACS Appl. Mater. Interfaces 2 (2010) 2385–2392.
[20] W.L. Ong, Y. Lim, J.L. Ting Ong, G.W. Ho, J. Mater. Chem. A 3 (2015) 6509–6516.

[21] L. Liu, W. Yang, W. Sun, Q. Li, J.K. Shang, ACS Appl. Mater. Interfaces 7 (2015) 1465–1476.
[22] M. Zhang, C. Shao, P. Zhang, C. Su, X. Zhang, P. Liang, Y. Sun, Y. Liu, J. Hazard. Mater. 225–226 (2012) 155–163.
[23] J. Tian, Y. Sang, G. Yu, H. Jiang, X. Mu, H. Liu, Adv. Mater. 25 (2013) 5075–5080.
[24] A. Fujishima, Nature 238 (1972) 37–38.
[25] J.S. Lee, K.H. You, C.B. Park, Adv. Mater. 24 (2012) 1084–1088.
[26] W. Zhou, Z. Yin, Y. Du, X. Huang, Z. Zeng, Z. Fan, H. Liu, J. Wang, H. Zhang, Small 9 (2013) 140–147.
[27] Y. Ma, X. Wang, Y. Jia, X. Chen, H. Han, C. Li, Chem. Rev. 114 (2014) 9987–10043.
[28] W. Guo, F. Zhang, C. Lin, Z.L. Wang, Adv. Mater. 24 (2012) 4761–4764.
[29] J. Pan, G. Liu, G.Q.M. Lu, H. Cheng, Angew. Chem. Int. Ed. 50 (2011) 2133–2137.
[30] H.G. Yang, C.H. Sun, S.Z. Qiao, J. Zou, G. Liu, S.C. Smith, H.M. Cheng, G.Q. Lu, Nature 453 (2008) 638–641.
[31] A. Selloni, Nat. Mater. 7 (2008) 613–615.
[32] J. Ananpattarachai, S. Seraphin, P. Kajitvichyanukul, Environ. Sci. Pollut. R. 23 (2016) 3884–3896.
[33] Y. Guan, N. Zhao, B. Tang, Q. Jia, X. Xu, H. Liu, R.I. Boughton, Chem. Commun. 49 (2013) 11524.
[34] Y. Wang, G. Du, H. Liu, D. Liu, S. Qin, J. Wang, X. Tao, M. Jiang, Z.L. Wang, J. Nanosci. Nanotechnol. 9 (2009) 2119–2123.
[35] L. Pan, H. Huang, C.K. Lim, Q.Y. Hong, M.S. Tse, O.K. Tan, RSC Adv. 3 (2013) 3566–3571.
[36] K. Yang, Y. Dai, B. Huang, J. Phys. Chem. C 111 (2007) 18985–18994.
[37] R. Daghrir, P. Drogui, D. Robert, Ind. Eng. Chem. Res. 52 (2013) 3581–3599.
[38] V. Pfeifer, P. Erhart, S. Li, K. Rachut, J. Morasch, J. Brötz, P. Reckers, T. Mayer, S. Rühle, A. Zaban, J. Phys. Chem. Lett. 4 (2013) 4182–4187.
[39] W. Zhou, H. Liu, R.I. Boughton, G. Du, J. Lin, J. Wang, D. Liu, J. Mater. Chem. 20 (2010) 5993.
[40] Z. Zhao, J. Tian, Y. Sang, A. Cabot, H. Liu, Adv. Mater. 27 (2015) 2557–2582.
[41] T. Luttrell, S. Halpegamage, J. Tao, A. Kramer, E. Sutter, M. Batzill, Sci. Rep.-UK 4 (2014).
[42] A. Sclafani, J.M. Herrmann, J. Phys. Chem. 100 (1996) 13655–13661.
[43] J. Zhang, Q. Xu, Z. Feng, M. Li, C. Li, Angew. Chem. Int. Ed. 120 (2008) 1790–1793.
[44] Q. Li, J. Zhang, B. Liu, M. Li, R. Liu, X. Li, H. Ma, S. Yu, L. Wang, Y. Zou, Z. Li, B. Zou, T. Cui, G. Zou, Inorg. Chem. 47 (2008) 9870–9873.
[45] S. Yoon, E. Lee, A. Manthiram, Inorg. Chem. 51 (2012) 3505–3512.
[46] C. Wang, X. Zhang, Y. Zhang, Y. Jia, J. Yang, P. Sun, Y. Liu, J. Phys. Chem. C 115 (2011) 22276–22285.
[47] J. Wang, J. Sun, X. Bian, Mat. Sci. Eng.: A 379 (2004) 7–10.
[48] Y. Wang, G. Du, H. Liu, D. Liu, S. Qin, N. Wang, C. Hu, X. Tao, J. Jiao, J. Wang, Z.L. Wang, Adv. Funct. Mater. 18 (2008) 1131–1137.
[49] T. He, F. Pan, Z. Xi, X. Zhang, H. Zhang, Z. Wang, M. Zhao, S. Yan, Y. Xia, J. Phys. Chem. C 114 (2010) 9234–9238.
[50] K. Kiatkittipong, C. Ye, J. Scott, R. Amal, Cryst. Growth Des. 10 (2010) 3618–3625.
[51] X. Chen, S.S. Mao, Chem. Rev. 107 (2007) 2891–2959.
[52] H.G. Yang, G. Liu, S.Z. Qiao, C.H. Sun, Y.G. Jin, S.C. Smith, J. Zou, H.M. Cheng, G.Q. Lu, J. Am. Chem. Soc. 131 (2009) 4078–4083.
[53] C. Wang, X. Zhang, Y. Zhang, Y. Jia, J. Yang, P. Sun, Y. Liu, J. Phys. Chem. C 115 (2011) 22276–22285.
[54] I.S. Cho, Z. Chen, A.J. Forman, D.R. Kim, P.M. Rao, T.F. Jaramillo, X. Zheng, Nano Lett. 11 (2011) 4978–4984.
[55] Y.V. Kolen'Ko, A.A. Burukhin, B.R. Churagulov, N.N. Oleynikov, Mater. Lett. 57 (2003) 1124–1129.
[56] H.B. Wu, H.H. Hng, X.W.D. Lou, Adv. Mater. 24 (2012) 2567–2571.
[57] H. Li, Y. Wang, G. Chen, Y. Sang, H. Jiang, J. He, X. Li, H. Liu, Nanoscale 8 (2016) 6101–6109.
[58] W. Wen, J. Wu, Y. Jiang, S. Yu, J. Bai, M. Cao, J. Cui, Sci. Rep. 5 (2015) 11804.
[59] L. Lai, J. Wu, J. Mater. Chem. A 3 (2015) 15863–15868.
[60] J. Bai, W. Wen, J. Wu, CrystEngComm 18 (2016) 1847–1853.
[61] N. Wu, J. Wang, D.N. Tafen, H. Wang, J. Zheng, J.P. Lewis, X. Liu, S.S. Leonard, A. Manivannan, J. Am. Chem. Soc. 132 (2010) 6679–6685.
[62] W. Zhou, L. Gai, P. Hu, J. Cui, X. Liu, D. Wang, G. Li, H. Jiang, D. Liu, H. Liu, J. Wang, CrystEngComm 13 (2011) 6643.
[63] R. Asahi, Y. Taga, W. Mannstadt, A.J. Freeman, Phys. Rev. B 61 (2000) 7459.
[64] Y. Sang, H. Liu, A. Umar, ChemCatChem 7 (2015) 559–573.
[65] W.E. Kaden, T. Wu, W.A. Kunkel, S.L. Anderson, Science 326 (2009) 826–829.
[66] N. Serpone, A. Salinaro, A.V. Emeline, S. Horikoshi, H. Hidaka, J. Zhao, Photochem. Photobiol. Sci. 1 (2002) 970.
[67] C.H. Kwon, H. Shin, J.H. Kim, W.S. Choi, K.H. Yoon, Mater. Chem. Phys. 86 (2004) 78–82.
[68] Q. Xiang, J. Yu, W. Wang, M. Jaroniec, Chem. Commun. 47 (2011) 6906–6908.
[69] G. Zhang, J. Zhang, M. Zhang, X. Wang, J. Mater. Chem. 22 (2012) 8083–8091.
[70] E. Grabowska, M. Diak, M. Marchelek, A. Zaleska, Appl. Catal. B: Environ. 156–157 (2014) 213–235.
[71] W. Zhou, G. Du, P. Hu, G. Li, D. Wang, H. Liu, J. Wang, R.I. Boughton, D. Liu, H. Jiang, J. Mater. Chem. 21 (2011) 7937.
[72] K. Sayama, K. Mukasa, R. Abe, Y. Abe, H. Arakawa, J. Photochem. Photobiol. A 148 (2002) 71–77.
[73] M.R. Hoffmann, S.T. Martin, W. Choi, D.W. Bahnemann, Chem. Rev. 95 (1995) 69–96.
[74] X. Chen, S. Shen, L. Guo, S.S. Mao, Chem. Rev. 110 (2010) 6503–6570.
[75] M.R. Hoffmann, S.T. Martin, W. Choi, D.W. Bahnemann, Chem. Rev. 95 (1995) 69–96.
[76] J. Tian, Y. Sang, Z. Zhao, W. Zhou, D. Wang, X. Kang, H. Liu, J. Wang, S. Chen, H. Cai, H. Huang, Small 9 (2013) 3864–3872.
[77] H. Chun, W. Yizhong, T. Hongxiao, Appl. Catal. B: Environ. 30 (2001) 277–285.
[78] B. Liu, A. Khare, E.S. Aydil, ACS Appl. Mater. Interfaces 3 (2011) 4444–4450.
[79] K. Pan, Y. Dong, W. Zhou, Q. Pan, Y. Yuan, X. Miao, G. Tian, Electrochim. Acta 88 (2013) 263–269.
[80] Z. Liu, X. Zhang, S. Nishimoto, M. Jin, D.A. Tryk, T. Murakami, A. Fujishima, Langmuir 23 (2007) 10916–10919.
[81] W. Li, C. Liu, Y. Zhou, Y. Bai, X. Feng, Z. Yang, L. Lu, X. Lu, K. Chan, J. Phys. Chem. C 112 (2008) 20539–20545.
[82] D. Yang, J. Zhao, H. Liu, Z. Zheng, M.O. Adebajo, H. Wang, X. Liu, H. Zhang, J.C. Zhao, J. Bell, Chem.- Eur. J. 19 (2013) 5113–5119.
[83] J. Lin, J. Shen, R. Wang, J. Cui, W. Zhou, P. Hu, D. Liu, H. Liu, J. Wang, R.I. Boughton, J. Mater. Chem. 21 (2011) 5106–5113.
[84] X. Yu, J. Zhang, Z. Zhao, W. Guo, J. Qiu, X. Mou, A. Li, J.P. Claverie, H. Liu, Nano Energy 16 (2015) 207–217.
[85] C. Sah, R. Noyce, W. Shockley, P. IRE 45 (1957) 1228–1243.
[86] C.W. Sohn, R.P. Smith, J.S. Kim, S.K. Noh, H. Choi, J. Leem, J. Korean Phys. Soc. 64 (2014) 1031–1035.
[87] Y. Yang, J. Gu, J.L. Young, E.M. Miller, J.A. Turner, N.R. Neale, M.C. Beard, Science 350 (2015) 1061–1065.
[88] B.J. Morgan, G.W. Watson, J. Phys. Chem. C 114 (2010) 2321–2328.
[89] L. Yang, S. Luo, Y. Li, Y. Xiao, Q. Kang, Q. Cai, Environ. Sci. Technol. 44 (2010) 7641–7646.
[90] C. Shifu, Z. Sujuan, L. Wei, Z. Wei, J. Hazard. Mater. 155 (2008) 320–326.
[91] G. Dai, J. Yu, G. Liu, J. Phys. Chem. C 115 (2011) 7339–7346.
[92] Y. Wang, Q. Wang, X. Zhan, F. Wang, M. Safdar, J. He, Nanoscale 5 (2013) 8326–8339.
[93] D. Sarkar, C.K. Ghosh, S. Mukherjee, K.K. Chattopadhyay, ACS Appl. Mater. Interfaces 5 (2013) 331–337.
[94] H. Shu, J. Xie, H. Xu, H. Li, Z. Gu, G. Sun, Y. Xu, J. Alloy Compd. 496 (2010) 633–637.
[95] W. Wang, X. Huang, S. Wu, Y. Zhou, L. Wang, H. Shi, Y. Liang, B. Zou, Appl. Catal. B: Environ. 134 (2013) 293–301.
[96] D. Wang, W. Zhou, P. Hu, Y. Guan, L. Chen, J. Li, G. Wang, H. Liu, J. Wang, G. Cao, H. Jiang, J. Colloid Interfaces Sci. 388 (2012) 144–150.
[97] J.L. Freeouf, J.M. Woodall, Appl. Phys. Lett. 39 (1981) 727–729.
[98] W. Zhou, D. Wang, H. Liu, J. Wang, Sci. Adv. Mater. 6 (2014) 538–544.
[99] W. Zhou, Y. Guan, D. Wang, X. Zhang, D. Liu, H. Jiang, J. Wang, X. Liu, H. Liu, S. Chen, Chem. —Asian J. 9 (2014) 1648–1654.
[100] T. Jiang, C. Jia, L. Zhang, S. He, Y. Sang, H. Li, Y. Li, X. Xu, H. Liu, Nanoscale 7 (2015) 209–217.
[101] D. Zhao, Y. Yu, H. Long, Y. Cao, Appl. Surf. Sci. 315 (2014) 247–251.
[102] W. Zhou, H. Liu, J. Wang, D. Liu, G. Du, J. Cui, ACS Appl. Mater. Inter. 2 (2010) 2385–2392.
[103] W. Zhou, H. Liu, J. Wang, D. Liu, G. Du, S. Han, J. Lin, R. Wang, Phys. Chem. Chem. Phys. 12 (2010) 15119.
[104] H. He, Y. Miao, Y. Du, J. Zhao, Y. Liu, P. Yang, Ceram. Int. 42 (2016) 97–102.
[105] J. Tian, X. Hu, N. Wei, Y. Zhou, X. Xu, H. Cui, H. Liu, Sol. Energy Mater. Sol. Cells 151 (2016) 7–13.
[106] G. Chen, S. Ji, Y. Sang, S. Chang, Y. Wang, P. Hao, J. Claverie, H. Liu, G. Yu, Nanoscale 7 (2015) 3117–3125.
[107] N.K. Eswar, P.C. Ramamurthy, G. Madras, Photochem. Photobiol. Sci. 14 (2015) 1227–1237.
[108] Y. Ao, J. Xu, P. Wang, C. Wang, J. Hou, J. Qian, Y. Li, Colloid Surf. A 487 (2015) 66–74.
[109] Y. Sang, Z. Zhao, M. Zhao, P. Hao, Y. Leng, H. Liu, Adv. Mater. 27 (2015) 363–369.
[110] Z. Li, F. Shi, T. Zhang, H. Wu, L. Sun, C. Yan, Chem. Commun. 47 (2011) 8109.
[111] W. Qin, D. Zhang, D. Zhao, L. Wang, K. Zheng, Chem. Commun. 46 (2010) 2304.
[112] F. Wang, Y. Han, C.S. Lim, Y. Lu, J. Wang, J. Xu, H. Chen, C. Zhang, M. Hong, X. Liu, Nature 463 (2010) 1061–1065.
[113] G.S. Yi, G.M. Chow, Adv. Funct. Mater. 16 (2006) 2324–2329.
[114] X. Chen, L. Liu, Y.Y. Peter, S.S. Mao, Science 331 (2011) 746–750.
[115] J. Tian, P. Hao, N. Wei, H. Cui, H. Liu, ACS Catal. 5 (2015) 4530–4536.
[116] G. Wang, B. Huang, X. Ma, Z. Wang, X. Qin, X. Zhang, Y. Dai, M. Whangbo, Angew. Chem. Int. Ed. 52 (2013) 4810–4813.
[117] W. Gao, W. Liu, Y. Leng, X. Wang, X. Wang, B. Hu, D. Yu, Y. Sang, H. Liu, Appl. Catal. B: Environ. 176–177 (2015) 83–90.
[118] J. Tian, Y. Leng, Z. Zhao, Y. Xia, Y. Sang, P. Hao, J. Zhan, M. Li, H. Liu, Nano Energy 11 (2015) 419–427.
[119] X. Pan, M. Yang, X. Fu, N. Zhang, Y. Xu, Nanoscale 5 (2013) 3601.
[120] M. Setvín, U. Aschauer, P. Scheiber, Y. Li, W. Hou, M. Schmid, A. Selloni, U. Diebold, Science 341 (2013) 988–991.
[121] S. Li, J. Qiu, M. Ling, F. Peng, B. Wood, S. Zhang, ACS Appl. Mater. Interfaces 5 (2013) 11129–11135.
[122] T.L. Thompson, J.T. Yates, Top. Catal. 35 (2005) 197–210.
[123] H. Zhang, H. Huang, H. Ming, H. Li, L. Zhang, Y. Liu, Z. Kang, J. Mater. Chem. 22 (2012) 10501.
[124] X. Zhang, H. Huang, J. Liu, Y. Liu, Z. Kang, J. Mater. Chem. A 1 (2013) 11529.

Xiaofei Zhang obtained his B.S. degree from Shandong University in 2015. Currently, he studies as a master student in Prof. Hong Liu's group in State Key Laboratory of Crystal Materials, Shandong University, China since September 2015. His research interests are synthesis of nanomaterials and their photocatalysis application.

Dr. Yuanhua Sang obtained his B.S. degrees at Shandong University in China in 2007 and completed his Ph.D. with Prof. Hong Liu at Shandong University in July 2012. Now, he works as a lecturer in State Key Laboratory of Crystal Materials, Shandong University, China. His research interests are structure and property investigation of inorganic crystal materials with neutron and x-ray diffraction, functional materials, and materials for solar light conversion.

Yana Wang obtained her B.S. degrees at Shandong University in China in 2013. Now, she studies as a master student in Prof. Hong Liu's group in State Key Laboratory of Crystal Materials, Shandong University, China since September 2013. Her research interests are synthesis of nanomaterials and their performance improvement in photocatalytic application.

Dr. Hong Liu is professor in State Key Laboratory of Crystal Materials, Shandong University. He received his PhD degree in 2001 from Shandong University (China). His current research is focused mainly on nonlinear crystal growth, chemical processing of nanomaterials for energy related applications including photocatalysis, tissue engineering, especially the interaction between stem cell and nanostrucuture of biomaterials.

Baishan Liu obtained his B.S. degrees at China University of Petroleum in 2001. He is the manager of Jiaxing Rejdue Environmental Technology Co., Ltd. His interest focusing on materials synthesis and facility design in environmental protection and waste-water treatment. Now, he is working on the design and fabrication of waste-water treatment facility combining biochemical treatment and photocatalysis.